Title

DIFFUSIVE PHENOMENA. REFLECTED IN THE CHARGE and ANGULAR DISTRIBUTIONS OF I, 2 fe, Ar, Kr INDUCED REACTIONS

Author

Moretto, L.G.

Publication Date

1976-03-01

Invited paper to the "Symposium on Macroscopic Features of Heavy Ion Collision," ANL, Argonne, IL., April 1-3, 1976

LBL-5006
c.1

DIFFUSIVE PHENOMENA REFLECTED IN THE CHARGE AND ANGULAR DISTRIBUTIONS OF N, Ne, Ar, Kr INDUCED REACTIONS

L. G. Moretto and J. S. Sventek

March 1976

Prepared for the U.S. Energy Research and Development Administration under Contract W-7405-ENG-48

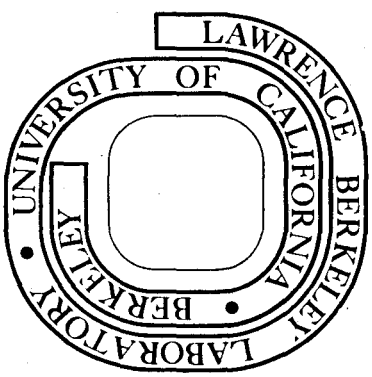

LBL-5006
c.1

DISCLAIMER

LBL-5006

DIFFUSIVE PHENOMENA REFLECTED IN THE CHARGE AND ANGULAR DISTRIBUTIONS OF N, Ne, Ar, Kr INDUCED REACTIONS*

L. G. Moretto** and J. S. Sventek

Department of Chemistry
and
Lawrence Berkeley Laboratory
University of California
Berkeley, California 94720

ABSTRACT

The presence of diffusion processes in heavy ion reactions is argued on a theoretical ground by pointing out the limitation of a Lagrangian approach to the time dependent processes. The Master Equation is used to describe the diffusion of the probability distribution along the mass asymmetry coordinate. Calculations of the probability distributions as a function of time have been performed for many heavy ion reactions. Experimental evidence of diffusion is shown to exist in the charge and angular distributions associated with a large number of heavy ion reactions. It is shown that the deep inelastic processes occurring in lighter systems, and quasi fission observed for heavier systems can be interpreted in terms of the very same mechanism. A comparison between the theoretical calculations and the experimental data is shown.

* Work performed under the auspices of the U.S. Energy Research and Development Adm.
** Sloan Fellow 1974 - 1976.

INTRODUCTION

In retrospect, looking at the state of nuclear physics before the renewed interest in heavy ion reactions, one appreciates the fact that relaxation processes, while not quite unknown, represented a small though reasonably well documented chapter. Such a chapter contained, for instance, doorway states, giant resonances of various multipolarities, pre-equilibrium emission of particles, etc.

Yet, the complex series of phenomena uncovered by heavy ion reactions, which now appears to be due to relaxation processes associated with various collective modes, caught us by surprise. In this new light, nuclear reactions induced by conventional projectiles seem to be even more polarized, since their interaction time covers only the extremes of a wide time range that is now being filled by the heavy ion reactions. On the one hand one has the direct reactions, involving times comparable to one single particle or collective period, and exciting but a few nuclear degrees of freedom, with the consequent small degree of inelasticity. On the other hand, one has the long-lived compound nucleus whose internal modes are in statistical equilibrium and for which all the information regarding time dependent processes is obliterated by thermal death. From these considerations it is now being realized that the chapter of nuclear physics covering relaxation processes, and time dependent processes in general, still remains to be written.

The first and best advertized process observed in heavy ion reactions is that associated with a dramatic loss in kinetic energy experienced in the target projectile collision.[1-4] Names like deep inelastic, strongly damped, or relaxed processes have been associated with the usually large fraction of the cross section where an extreme loss of kinetic energy is

observed. The mechanisms by which the energy is dissipated and presumably transferred into the internal degrees of freedom has been discussed at the microscopic level by various authors and is not completely clear as yet.[5-7] Phenomenologically, macroscopic quantities like viscosity or friction coefficients have been introduced in a classical Lagrangian formalism in order to describe the kinetic energy dissipation.[8-13]

In most processes observed in heavy ion reactions, a short-lived intermediate structure manifests itself which we have chosen to call "intermediate complex" in analogy with chemical reactions.[14-15] Such an intermediate complex seems to be fully thermalized in so far as the entrance channel kinetic energy is concerned, and completely equilibrated with respect to all but the slowest degrees of freedom, like the mass asymmetry mode. We have occasionally used for it the shape of two spherical liquid drops in contact. This definition should be taken only as a tentative and qualitative description of the intermediate system.

A few essential features point towards the equilibrium aspects of the intermediate complex, like the completely thermalized spectra of the relaxed cross section. The charge-to-mass ratio of the fragments also seems to be be equilibrated at fixed mass asymmetry as suggested by recent experiments.[16-17]

No information regarding the equilibration (or the lack of it) of higher multipole degrees of freedom is available as yet.

Strong evidence is available for the lack of equilibration along the mass asymmetry coordinate which appears to be the slowest mode. This evidence comes from the detailed study of the charge distribution of the particles emitted in many heavy ion reactions and from their angular distribution.[18-24] The dependence of the angular distributions upon the atomic number of the emitted fragments suggests that the system tends to equilibrium

in the mass asymmetry degree of freedom by means of a diffusion mechanism.[14,19] The analysis of the angular distributions and of the charge distributions in terms of the Master Equation has led to the determination of the lifetimes as well as of the diffusion coefficient.[14,19-24] Similar analysis of the charge distribution and kinetic energy distributions in the quasi-elastic region have been attempted in terms of the Fokker-Planck equation.[25-26] It seems now that the present body of evidence points towards a picture where diffusion is the prevailing process. In other words, it appears that a strong coupling limit between collective and intrinsic modes is established in preference to weak coupling which could be more simply described in terms of classical motion in collective phase space.

It is the purpose of this paper to analyze a suitably chosen body of experimental evidence collected by our group at Berkeley in order to show the extent to which the diffusion mechanism can be established in the relaxation along the mass asymmetry mode.

In the first section, the problem of time dependent processes in nuclei is qualitatively discussed and the various theoretical approaches to it are briefly analyzed. In particular the role of the internal degrees of freedom is stressed and their connection with the diffusion mechanism is pointed out. The Master Equation is then discussed and applied to the problem of relaxation along the mass asymmetry coordinate. Probability distributions are obtained for some of the systems studied experimentally and are discussed in terms of the potential energy curves. A general equation describing the angular distributions as a function of Z is presented.

In the second section a brief discussion on the experimental kinetic energy distributions is given and the extent to which the kinetic energies are thermalized is illustrated.

In the third section a detailed analysis of the Z distribution is presented for the reactions Ag+N, Ne, Ar, Kr; Au+Ar, Kr; Ta+Kr. The evidence for lack of equilibration in the mass asymmetry mode is discussed in terms of the potential energies and of the decay times.

The fourth section deals with the angular distributions for the above reactions as a function of the Z of the fragment. The most direct evidence of the diffusion process is found in the transition from side peaking to forward peaking as one moves away in Z from the projectile in the reactions Au+Kr and Ta+Kr. Examples of theoretical angular distributions and a comparison with the experimental data are shown.

SECTION I: *Theoretical Considerations on the Description of Time Dependent Processes in Nuclei.*

The Ingredients for a Collective Description of the Nucleus-Nucleus Interaction

As the experimental time-dependent processes involve collective degrees of freedom, it seems natural to investigate the various quantities which may enter in a theoretical description as a function of a suitably chosen set of collective coordinates. The liquid drop model has made the mapping of the potential energy quite easy for connected shapes. Furthermore, the proximity force approach[27] or similar treatments[28] nicely take care of the interaction between separated or slightly overlapping nuclei.

The potential energy, complemented by shrewd guesses about the inertia matrix, allows one to treat the problem in terms of classical dynamics. The experimentally observed dissipation of large amounts of kinetic energy associated with the entrance channel suggests the introduction of frictional or viscous forces in order to complete the dynamical description of the system.[8-13]

The Lagrangian Temptation

One can try to describe the time evolution of the system by means of the Lagrangian equation of motion:

$$\frac{d}{dt}\frac{\partial L}{\partial \dot{q}_i} = \frac{\partial L}{\partial q_i} - \frac{\partial F}{\partial \dot{q}_i}$$

where L is the Lagrangian expressed in terms of the generalized coordinates q_i and velocities $\dot{q}_i$:

$$L = \frac{1}{2}\sum_{i,j} m_{ij}\,\dot{q}_i\,\dot{q}_j - V(q_1,q_2,q_3\ldots)$$

and F is the dissipation function

$$F = \frac{1}{2}\sum_{i,j} a_{ij}\,\dot{q}_1\,\dot{q}_j$$

For a given set of initial conditions, the equations of motion can be solved and a trajectory in coordinate space can be obtained. Better yet, one has a more complete appreciation of the dynamic evolution of the system by considering the trajectory in the collective phase space (p_i,q_i).

Unfortunately, in the approach outlined above, one has tacitly dismissed (or covered up) the fact that the collective phase space is but a small section of the overall phase space. The only lip service paid to the existence of such an underworld of degrees of freedom is the dissipation function, which relegates the function of these degrees of freedom to a dumping ground for the energy in the collective motion without any feedback. It is easy to show that the role of the intrinsic degrees of freedom is in fact more active and substantial.

The Revenge of the Underworld, or the Effect of Internal Degrees of Freedom

If we reconsider the collective phase space as a section of the total phase space, one immediately appreciates the possible weakness of the Lagrangian approach. Let us consider an ensemble of systems, all with the same initial conditions in the collective coordinates and momenta, but with unspecified (random) initial conditions for the intrinsic degrees of freedom. When projected in the collective phase space, the trajectories associated with each of the systems in the ensemble have their origin in common, but tend to diverge from one another as the time goes on, because the set of the overall initial condition is different for each system. In other words, the time evolution of a single system is not completely predictable in so far as the initial conditions are not completely specified. Thus one is forced to abandon the deterministic description of a single system and is led to consider a statistical description of an ensemble of systems in terms of a time dependent probability distribution in the collective phase space.

Despite these considerations it is well known that in most cases the Lagrangian approach, modified to include the dissipation function is quite adequate, and that fluctuations about the mean value in the observed dynamical quantities are negligible. Therefore one must establish under which conditions fluctuations can be neglected.

General Condiderations About Statistical Fluctuations

Let us consider first a macroscopic fluid at equilibrium. For such a system, the fluctuations about its equilibrium point along any collective coordinate involve an amount of energy of the order of kT. This compares with the total energy E of the system which is of the order NkT, where N is the total number of degrees of freedom. This means that the r.m.s. fluctuation along a collective coordinate is of order $\sqrt{E/aN}$,

where a is the stiffness coefficient; for $N \simeq 10^{23}$ this fluctuation is small indeed unless $a = 0$. This is why we do not commonly observe sizeable fluctuations in the shape of ordinary objects at thermal equilibrium. In a nucleus, N is of the order of a few hundred and further reduced by the Pauly principle to $N_{eff} = N \frac{T}{\varepsilon_F}$, where ε_F is the Fermi energy and T is the nuclear temperature. For typical temperatures of a few MeV, N_{eff} is of the order of few tens. Thus very sizeable fluctuations are to be expected along the nuclear collective modes. Furthermore, since significant variations of the potential energy along a nuclear collective coordinate are of the order of a few MeV, it follows that the equilibrium statistical distribution along nuclear coordinates may be so complicated that it does not lend itself to a description in terms of a rapidly converging moment expansion.

Now let us come back to the dynamical problem. An initially cold macroscopic system with an assigned initial kinetic energy frictionally dissipates such an energy, which is taken up by the internal degrees of freedom. Since the specific heat $C_v \to \infty$, the ratio kT/E_{kin} is extremely small and the feedback from the underworld is negligible. As the system loses energy, it moves toward an equilibrium position following a well defined trajectory and, once it reaches it, will stay there. A Lagrangian treatment is perfectly adequate for such a system. For the nucleus, things are different. As the initial kinetic energy is transferred to the internal degrees of freedom, the temperature quickly rises to values comparable with the remaining kinetic energy. The fluctuations are now so sizeable that they severely perturb the collective motion of the system in a random fashion. An ensemble of nuclei will therefore follow trajectories which rapidly diverge, generating an ever more complex distribution in phase space which, in time, will merge into the broad equilibrium distribution.

In conclusion, strong viscous forces associated with small heat capacities will generate a sizeable dispersion about a Lagrangian trajectory.

The Master Equation as a Viable Treatment of Diffusion

A treatment which describes the time evolution of a probability distribution along a given coordinate is offered by the Master Equation. If $\phi(x,t)$ is the probability distribution in x at time t, its time evolution is given by

$$\dot{\phi}(x,t) = \int dx' \, \lambda(x,x')[\phi(x',t)\rho(x) - \phi(x,t)\rho(x')]$$

where $\lambda(x,x')$ is a microscopic transition probability and $\rho(x)$, $\rho(x')$ are the density of states associated with the collective variable at x,x'. By expanding ϕ and ρ in terms of $(x-x')$ and retaining terms up to second order, one obtains the Fokker-Planck equation:

$$\dot{\phi}(x,t) = \frac{\partial}{\partial x}[C_1(x)\phi(x,t)] + \frac{\partial^2}{\partial x^2}[C_2(x)\phi(x,t)] \, .$$

In this expression, C_1 and C_2 are the "drift" and the "spread" coefficients which can be related to the moments of the transition probability $\mu_n = \int dx' \, \lambda(x,x') \frac{(x-x')^n}{n!}$. The equation in very transparent. If ϕ is a Gaussian, the first term translates the Gaussian along x and the second term increases its width.

Application of the Master Equation

We have applied the Master Equation to the problem of diffusion along the mass asymmetry coordinate.[14] Let $\phi(Z,t)$ be the probability distribution associated with a configuration of two touching fragments, one of which has atomic number Z (we assume equilibration in the neutron-to-proton ratio and we label the asymmetry by Z since this is the quantity we measure

for each fragment). The Master Equation can then be written as:

$$\dot{\phi}(Z,t) = \sum_{Z'} \lambda_{ZZ'}(\phi_Z \rho_Z - \phi_Z \rho_{Z'})$$

where $\lambda_{ZZ'} = \lambda_{Z'Z}$ is the microscopic transition probability, ρ_Z and $\rho_{Z'}$ are the level densities associated with the asymmetries Z and Z'. The latter quantities can be written as

$$\rho_Z = \rho(E - V_Z) = \rho(E) e^{-V_Z/T}$$

where V_Z is the potential energy (including the rotational energy) of the intermediate complex with asymmetry Z; $\rho(x)$ is the nuclear level density; and the nuclear temperature T is given by: $T^{-1} = \left.\frac{\partial \ell n \rho}{\partial x}\right|_{x=E}$. The Master Equation can be rewritten as:

$$\dot{\phi}(Z,t) = \kappa \sum_{Z'} \frac{\rho(E) f_{ZZ'}}{(\rho_Z \rho_{Z'})^{1/2}} \left(\phi_{Z'} e^{-V_Z/T} - \phi_Z e^{-V_{Z'}/T} \right)$$

where we have set $\lambda_{ZZ'} = \kappa f_{ZZ'}/(\rho_Z \rho_{Z'})^{1/2}$ and $f_{ZZ'}$ is a form-factor equal to the area of contact of the two fragments in the intermediate complex. The sum over Z' can be limited to the values $Z' = Z \pm 1$ which implies an independent particle model and an uncorrelated transfer of nucleons from one side to the other of the intermediate complex.

Calculations of the probability distributions have been performed for some of the reactions studied experimentally. The key quantity that must be known is the potential energy of the intermediate complex as a function of Z. These potential energies have been calculated by assuming that the intermediate complex can be approximated by two touching liquid drop spheres. Examples of such calculations are shown in Figs. 1 through 4,

together with contour maps of the probability distribution as a function of time. In Fig. 1 the case of Ag+ ^{20}Ne at 252 MeV bombarding energy and $\ell = 0$ is considered. Since the injection point is to the left of the Businaro-Gallone peak, the probability distribution drifts rapidly toward low Z's. It also spreads quite rapidly due to the flattening of the effective potential V/T caused by the high temperature and, as the time progresses, more symmetric configurations are populated.

The case shown in Fig. 2 is the same as in Fig. 1 but for $\ell = 100$. In this case the injection point is to the right of the Businaro-Gallone peak, (notice the splitting of the Businaro-Gallone peak in two components) and the distribution dramatically drifts towards symmetry although the spread of the distribution populates the low Z's even more rapidly.

These examples, together with those shown in Figs. 3 and 4, will be discussed later when the experimental data for the corresponding reactions will be considered. For the moment it suffices to observe that:

i) The diffusion process depends strongly upon the potential energy and that rapid variations in potential energies are seen for various ℓ waves in the same reaction.

ii) The high temperatures prevailing in these reactions allow for a substantial spread of the distributions, so that a Lagrangian approach would miss essential aspects of the time-dependent process.

Since our ultimate goal is to obtain angular distributions as a function of Z, we have to combine the time-dependent probability distributions with the dynamics in the other degrees of freedom. If we assume the intermediate complex lives a time t after formation, we can write an expression

for the classical deflection function (θ), which is now a function of time. If the probability for the complex to survive a time t for a given impact parameter is T(t;b), we can write:

$$\frac{\partial^2\sigma}{\partial\Omega\ \partial t}\ (Z,\theta,t) = \sum_{\forall b} b\ P(b)\ T(t;b) \frac{\phi(Z,b,t)}{\sin\theta \left|\frac{d\theta}{db}\right|}$$

where P(b) is the probability that such an impact parameter be associated with a relaxed process; the sum is extended over those impact parameters yielding a fragment Z at the angle θ after time t.

The differential cross section can now be evaluated as:

$$\frac{d\sigma}{d\Omega}\ (Z,\theta) = \int_0^\infty dt \quad \frac{\partial^2\sigma}{\partial\Omega\ \partial t}\ (Z,\theta,t).$$

Examples of these calculations are shown in Figs. 24, 25 and 26.

SECTION 2: *Brief Comments on the Kinetic Energies*

The kinetic energy spectra in heavy ion reactions systematically present two components: A high energy component, genetically traceable to the energy of the incoming beam and thus commonly called "quasi-elastic"; and a low energy component, indistinguishable in many respects from a compound nucleus spectrum, called relaxed or deep inelastic or strongly damped. The first of the labels is perhaps more daring because it implies a "complete" thermalization of the spectrum, the second and the third are equivalent but noncommital as to the completeness of the thermalization process.

Some examples of the kinetic energy spectra can be seen in Fig. 5, where both components can be seen. It should be remarked that, in line with its more "direct" nature, the quasi-elastic component is visible close to the grazing angle and for fragments close in Z to the projectile, while

the relaxed component is observed at all angles for all fragments. There will be more opportunity to appreciate the features of the kinetic energy distributions in some contour maps of the differential cross section $\partial^2\sigma/\partial E\,\partial\theta$ which will be discussed below for different reasons. However it is difficult to resist the temptation to show Fig. 6 obtained from the reaction Au+Ar,[23] which can be compared with that made famous by Dr. Wilczynski.[29] In this figure a cross section ridge is seen to move from the grazing angle towards 0° while the energy is decreasing due to frictional losses. Such a pattern vividly suggests partial orbiting with the trajectory moving from positive to negative angles. A comparison with similar plots for the reaction Au + Kr [24] (Fig. 23) shows that in the latter case no orbiting is evident and that the trajectories are confined either to the left or to the right hemisphere, without even crossing the 0° plane. Since we are particularly interested in the behavior of the relaxed component of the cross section, some general features of it should be given. In Fig. 7 the most probable center of mass kinetic energies and the associated widths are presented for the reaction Au + Kr as a function of the atomic number of the fragment. In the same figure, the fragment energies expected from Coulomb repulsion are also shown. No attempt to fit the data is made, therefore no correction for particle emission has been performed on the data, nor is the rotational energy accounted for in any way. Our main interest is in showing two points: a) the independence of the center of mass energy from angle; b) the essentially Coulombian origin of the kinetic energy.

SECTION 3: *The Charge Distributions*

At first sight, the charge distributions should reflect the extent to which relaxation along the mass asymmetry degree of freedom has progressed. And, in fact, this is true in the case of rather short lifetimes. In such case the decay occurs when the mass asymmetry degree of freedom is far from equilibration as in the reactions of Au and Ta + Kr (see Figs. 13 and 14, and compare with Figs. 1 to 4), for which the Z distributions peak at or about the projectile, and the lack of equilibration is immediately appreciated.

More complex is the case in which the lifetime of the intermediate complex is long enough to allow for a substantial relaxation along the mass asymmetry mode. With the disappearance of the projectile peak in the probability distribution, one loses the most visible indication of incomplete relaxation. Again, this can be clearly seen in the theoretical calculations shown in Figs. 1 through 4. The inspection of the individual Z distributions in the reactions Ag + N,[21] Ne,[22] Ar,[21] Kr[31] (Figs. 8-10, 12) and Au + Ar[23] (Fig. 11) shows various features which, at first sight, may be interpreted as equilibrium features. For instance, from the ridge line potential energies (Figs. 1-4) one can obtain a guess regarding the shape of the equilibrium Z distribution. It is possible to show that the Z distribution Y(Z) should behave as

$$Y(Z) = K(Z,\ell) \exp(-V_z/T)$$

where V_z is the ridge-line potential energy, T is the ridge-line temperature, and K is a quantity which should depend weakly on Z, on angular momentum ℓ and on the temperature. Consequently, regions of low potential energy should correspond to large cross sections and *vice versa*. This can be

verified in the case of Ag + N [20] and Ag + Ne [22] (Figs. 8,9) where large cross sections are seen for low Z's and low cross sections are seen for intermediate Z's, close to symmetry. Furthermore, the V_z/T effect can be observed in a number of cases as a general flattening of the Z distribution at higher bombarding energies. Yet, when these distributions obtained in different reactions are compared with one another, it becomes evident that they still bear information regarding the entrance channel asymmetry. For instance, the reactions Ag + N, [21] Ag + Ne, [22] Ag + Ar [21] (Figs. 8,9,10) should produce similar compound nuclei and should be characterized by similar ridge lines. However the experimental charge distributions show an excess cross section in the light Z region for the first reaction (Fig. 8) and an ever decreasing cross section with increasing Z. The second reaction also shows large cross sections at low Z's, decreasing with increasing Z up to Z 12 $\sim$ 14 followed by a slow increase of the cross section for higher Z's (Fig. 9). The third reaction instead does not show any large cross section at low Z's. Rather the cross section monotonically increases with Z (Fig. 10). The complete inversion of the charge distribution pattern from the N projectile to the Ar projectile may be attributed to the change in the entrance channel mass asymmetry. An inspection of the ridge energies and to the entrance channel mass asymmetry clearly illustrate the case (Figs. 1-4).

The injection point for Ag + N is found on a steep slope leading towards the lightest Z's. Thus one should expect a drift in the diffusion process in this direction, which is experimentally confirmed in the great abundance of light products.

In the case of Ag + Ne the injection point is very close to the top of the Businaro-Gallone mountain, perhaps slightly to the left, depending

upon the angular momentum (Figs. 1,2). Therefore the diffusion again proceeds to the left towards lighter products, but also toward the heavier products in the region of symmetry. This is shown in the diffusion patterns in Figs. 1b, 2b, and is confirmed by the experimental distributions which show high cross sections for small Z's and an increasing cross section with increasing Z toward the symmetric splitting.

In the case of Ag + Ar, the injection point is to the right of the Businaro-Gallone mountain (Fig. 3). Therefore the system diffuses more easily towards near symmetric configurations than toward very asymmetric configurations (see theoretical calculation in Fig. 3b). The experiment confirms such a theoretical explanation by showing a cross section monotonically increasing with Z.

Very little information is carried by the Au + Ar Z distributions, which are monotonically increasing with Z, with the exception of those measured close to the grazing angle where a sharp peak is observed at Z = 18. These large cross sections for Z's closest to the projectile are characterized by incompletely relaxed kinetic energy distributions.

Also for the reaction Ag + Kr [31] (Fig. 12) the Z distributions are monotonically increasing with Z as far as symmetry. In this case the injection asymmetry is only five atomic numbers away from symmetry and consequently it appears that the system has diffused at least that far. This, of course, does not imply by itself full equilibration, because neither the width nor the detailed shape of the distribution may be corresponding to those expected from complete relaxation.

In fact for all the distributions discussed so far, the best proof of incomplete equilibration is provided by the angular distributions, as will be discussed later.

Still, even after such a confirmation has been obtained, one still may worry about the extent to which real compound nucleus fission may contribute to the observed distributions. This is really a very serious problem because, as we have shown elsewhere, [14] even a $1/\sin\theta$ angular distribution does not guarantee a compound nucleus origin. This can be seen in the theoretical angular distributions shown in Fig. 25 where the limit of $1/\sin\theta$ is attained without even invoking the compound nucleus mechanism. It is conceivable that excitation functions as a function of Z may help to solve the mystery, but the available data are not sufficient to reach any conclusions as yet.

In contrast with the previously discussed reactions, the reactions induced by very heavy ions on heavy targets are characterized by charge distributions sharply peaked at, or close to, the projectile. This is the case for the two reactions which we have studied, namely Au + Kr [24] and Ta + Kr. [32] Their charge distributions (Fig. 13, 14) are remarkable in many ways. A fairly sharp peak at the Z of the projectile is seen in a narrow angular region corresponding to the peaking in angular distributions. At more forward and backward angles, the distributions are broader and it is difficult to decide where the distributions are actually peaking. This is particularly true of the second reaction. Since the sharply peaked charge distributions are characterized by kinetic energy distributions which are not fully relaxed, we have studied them for various windows in the kinetic energies. The results are seen in Fig. 15. At large kinetic energies, one observes narrow distributions, sharply peaked about $Z = 36$. As the kinetic energies become smaller, the distributions become broader although the most probable value seem to stay fixed at $Z = 36$. One is tempted to interpret these

features in terms of the diffusion model: Large kinetic energies and small widths in the charge distributions should be characteristic of short lives and *vice versa* (see Fig. 4a,4b).

Another remarkable feature observable in the charge distribution is the following: Sharp distributions are observed at intermediate angles; broader distributions are observed at forward angles; and even broader distributions are observed at the more backward angles (Figs. 13,14). In terms of the diffusion model, one can identify the sharpest charge distribution as the youngest because the system has had no time to diffuse to any great extent, while the broadest charge distributions can be identified as the oldest, because of the large amount of diffusion that appears to have occurred. The peculiar fact is that, moving from backward angles to forward angles, one encounters in the order: old distributions, young distributions and middle age distributions. The strange inversion of sequence seems to be due to an impact parameter effect. Let us assume that the lifetime of the intermediate complex decreases rapidly with the impact parameter, which is not unreasonable for a variety of reasons. Then one has for the decay angle the following very crude expression:

$$180^\circ - \theta = K_1 b + K_2 b(\tau_0 - \alpha b)$$

where the b is the impact parameter, $K_1 b$ is the angle between the beam direction and the line connecting the fragment centers, $K_2 b$ is the angular velocity, and $\tau_0 - \alpha b$ is the lifetime of a complex with impact parameter b. Therefore, the angle versus b curve is a parabola. This shows that the systems with small impact parameter are emitted at rather backward angles and are characterized by the longest lifetimes. Thus the Z distribution is expected

to be broad or in other words, "old". The systems with maximum impact parameter will be emitted at *intermediate* angles and, because of the shortest lifetime, will give rise to very young Z distributions. Finally, the systems with intermediate impact parameters will be emitted at the most forward angles and, because of their intermediate lifetime, will give rise to *middle-aged* angular distributions. This is well reproduced in the calculation leading to Fig. 26.

SECTION 4: *The Angular Distributions*

Reactions Induced by Ar and Lighter Projectiles and the Reaction Ag + Kr

The angular distributions, being so sensitive to short interaction times, gave the first alarm regarding the non compound nucleus nature of the relaxed cross section. This was especially true for the reactions induced by Ar and lighter projectiles, [1,14,18,19] or for that matter, for the reaction of Kr + Ag, [31] where the charge distributions gave only an ambiguous answer regarding the degree of equilibration along the mass asymmetry coordinate.

As can be seen in Figs. 16-20, the center of mass angular distributions appear to be generally forward peaked in these reactions, especially for fragments close in Z to the projectile.

This, by itself, is very significant in many respects. To begin with, there is some memory effect which couples entrance and exit channels. The intermediate complex can distinguish the forward from the backward direction in a way that a compound nucleus cannot, irrespective of its actual lifetime. The intermediate complex lifetime, of course, must be relatively short with respect to the mean rotational period; not too short though, otherwise the system could not rotate enough to cross the 0° line and would give rise to

a side peak; not too long, otherwise the angular distribution would become symmetrized about 90°.

The presence of a smaller backward peaking in some of the reaction products suggests that in a substantial fraction of the cases the rotation proceeds through zero towards the most backward negative angles, and perhaps even through 180°. Therefore, a qualitative guess would set the lifetime of the intermediate complex at a sizeable fraction of the mean rotational period.

Another implication of the forward peaking associated with relaxed cross sections is that the relaxation of the kinetic energy occurs on a time scale short both with respect to the rotational period as well as with respect to the mass asymmetry relaxation time. However, the most informative feature in the angular distributions in reactions induced by light projectiles and including the reaction Ag+Kr, is the dependence of the angular distribution upon the atomic number of the fragment. This effect is particularly visible in the reactions Ag+N [20] and Ag+Ne, [22] though it is present in all the other reactions. In *all* of these reactions, the forward peaking is stronger for fragments closer in Z to the projectile and decreases for fragments substantially removed from the projectile. This phenomenon finds its qualitative explanation in the increasing time lag, introduced by the diffusion process, in the population of configurations farther and farther removed in mass asymmetry from that associated with the target-projectile combination (injection asymmetry). In this way, fragments close in Z to the projectile are rapidly populated by the diffusion process (see Figs. 1-4) and can rapidly decay, thus generating a substantially forward-peaked angular distribution. Fragments farther removed in Z from the projectile are populated on a longer time scale, so that their decay time is delayed. Such

a delay allows the system to rotate for a longer time, which results in an increased tendency for the angular distribution to become more and more symmetric at about 90°.

This feature appears to various degrees in the various reactions. On the one hand one sees a very rapid symmetrization in Ag + Ne and Ag + N as one moves from the projectile to fragments four or five units *higher* in Z. On the other hand, in Ag + Ar [21] and even more in Ag + Kr, [31] one observes a very small decrease in the forward peaking as one moves from the projectile *down* in Z by as much as 10 to 20 units.

It appears that these variations in trends can be traced back to the effect of the potential energy upon the diffusion process. Let us first consider reactions like Ag + N and Ag + Ne. Both of these reactions are characterized by very sharply peaked angular distributions which rapidly become symmetrized as one moves above the Z of the projectile. For instance, in Ag + Ne the angular distribution for $Z = 15$ is already of the form $1/\sin\theta$. The reason for such an asymmetric behavior for fragments above or below in Z to the projectile can be readily appreciated by studying Figs. 1 and 2 where the potential energy of the intermediate complex is shown as a function of the Z of one of the fragments. The injection asymmetry for both of these systems for most of the ℓ waves is to the left of the Businaro-Gallone mountain, on a steep slope leading to extreme asymmetries. As a consequence, diffusion populates the lower Z's very rapidly because of the fast drift imposed by the steep potential energy, as illustrated by the theoretical calculations shown in Fig. 1b. This results in sharply forward peaked angular distributions. Conversely, the Z's above the projectile must rely for their population on the spreading uphill of the probability distribution,

which is clearly a much slower process. The result is a very rapid damping of the forward peaking as one moves above the Z of the projectile.

An intermediate situation if found in Ag + Ar. The injection asymmetry is now slightly to the right of the Businaro-Gallone peak (Fig. 2a). As is well illustrated by the theoretical calculation shown in Fig. 2b, the diffusion feels the rapid descent of the potential energy to the left of the Businaro-Gallone peak, even though the potential energy tends to drive the system towards symmetry. As a consequence, the low Z's are still populated rather early in time, though not as fast as in the previous cases. This gives rise to moderately forward peaked angular distributions becoming less sharply peaked as one moves towards smaller atomic numbers. The theoretical calculations shown in Figs. 24 and 25 reproduce the effects illustrated above both qualitatively and quantitatively.

An interesting feature is visible in the Au + Ar angular distributions (Fig. 19). In this reaction the injection asymmetry is found to be to the right of the Businaro-Gallone mountain, on a steep slope which drives the diffusion towards more symmetric configuration. Remarkably, the angular distributions remain forward peaked from $Z = 18$ to $Z = 29$, as many as eleven Z units above the projectile. In comparison, in the reactions Ag + N and Ag + Ne, the forward peaking disappears after only four to five atomic numbers above the projectile. Therefore the inversion of the drift in diffusion associated with an inversion in the slope of the potential energy with respect to the mass asymmetry seems to be well confirmed. The expected opposite effect of decreasing sharpness in the forward peaking for $Z < 18$ is not verified in the Au + Ar reaction. In fact quite a sharp forward peaking is observed for these products. Yet, differently from the fragments with $Z > 18$ whose kinetic

energy spectrum is fully relaxed, the fragments with $Z < 18$ have quite broad kinetic energy spectra with mean energies well above the expected values.

The Ag + Kr reaction is in all respects similar to the reactions observed with lighter projectiles (Fig. 20). The injection asymmetry is close to the symmetry minimum of the potential energy. The potential energy remains relatively flat over a fairly large range of asymmetries, making the spreading of the population towards atomic numbers smaller than the projectile a relatively fast process. Hence the moderately forward peaked angular distributions whose forward peaking slowly decreases as one moves towards the lighter fragments.

The Reactions Induced by Kr on Heavy Targets

When the reactions of Kr on heavy targets were first observed, [4,30] the sharpness of the mass distributions associated with the side peaking of the gross angular distributions appeared to be so extraordinary that they were thought to be a completely new mechanism, which was named quasi-fission. Yet, this process resembles the deep inelastic processes described above in many respects. In fact it became our ambition to prove that there is a continuous connection between the angular distributions observed in reactions induced by lighter projectiles (or by heavy projectiles on relatively light targets, like Ag + Kr), and the angular distributions observed in heavy projectile - heavy target reactions. We argued that the side peaking in the gross angular distribution of the products reflected a very short interaction time associated with a few Z's about the projectile. However, if one were to look at the angular distributions of individual Z's, one should observe

a progressive change towards forward peaking as one moves away from the Z of the projectile. In this spirit the study of the reactions Au, Ta + Kr was undertaken. The angular distributions for individual atomic numbers, resolved up to $Z \cong 50$ are shown in Figs. 21 and 22. The effect we were looking for indeed appears with astounding clarity. Close to $Z = 36$ a very sharp side-peak is observed (for the Z's closest to the projectile the separation of the quasi-elastic component appeared to be impossible so that some of the points close to the maximum of the peak are actually skipped). Such a side peak implies an interaction time so short that the intermediate complex does not have time enough to rotate past 0°. However, as one moves away in Z from the projectile, the progressively longer time delay imposed by diffusion allows the intermediate complex to reach closer to 0°, and eventually to reach past 0°. This results in a rapid filling-in of the angles close to 0°, which slowly transforms the side-peak first into a shoulder and later into a forward peak. In Au + Kr the side peak becomes a shoulder symmetrically about $Z = 36$, at $Z \cong 30$ and at $Z \cong 41$. The shoulder disappears around $Z = 24$ and $Z \cong 46$ where the angular distributions become forward peaked. Quite fittingly, in the reaction of Kr + Ta, the side peak is less pronounced and disappears earlier. The forward peaking then extends to the extreme Z's, both high and low which were accessible in the present measurement. The theoretical calculation shown in Fig. 26 reproduces in detail the experimental effects.

Thus in a single reaction, one observes the desired connection between the side-peaked and the forward-peaked angular distributions. Furthermore, the essential identity of the processes observed in reactions induced by light projectiles (characterized by forward peaked angular

distributions) and quasi-fission (characterized by both kinds of angular distributions) is proved. In general, the lifetimes of the intermediate complexes formed with heavy targets and projectiles are shorter than those of the lighter intermediate complexes due to larger Coulomb repulsion and centrifugal forces. Thus the connecting parameter between the two kinds of angular distributions is obviously the lifetime of the intermediate complex.

Conclusion

It has been the purpose of this paper to present a case for diffusion processes in heavy ion reactions. The case has been made on a qualitative theoretical ground by pointing out the deficiencies and limitations of a Lagrangian approach and by showing that the Master Equation naturally handles the drift and the spread in the probability distribution along a given collective coordinate. Evidence of diffusion-like phenomena has been produced in the form of a large amount of charge distributions and angular distributions obtained for a variety of heavy ion reactions. The lack of equilibration along the mass asymmetry degree of freedom of the intermediate complex has been shown and the Z dependence of the angular distribution has been interpreted in terms of the diffusion model. In particular, the essential unity of the deep-inelastic processes with their forward-peaked angular distribution and of quasi-fission with both forward-peaked and side-peaked angular distributions has been shown. Theoretical calculations based upon the diffusion model reproduce the experimental data in detail.

FIGURE CAPTIONS

Fig. 1. a) Potential energy of the intermediate complex for the reaction Ag + ^{20}Ne (two touching spheres) as a function of the Z of one of the two fragments. b) Probability distributions along the mass asymmetry coordinate as a function of time. The calculation has been performed for $\ell = 0$.

Fig. 2. Same as in Fig. 1 for $\ell = 100$.

Fig. 3. Same as in Fig. 1 for the reaction Ag + ^{40}Ar and $\ell = 100$.

Fig. 4. Same as in Fig. 1 for the reaction Au + ^{86}Kr and $\ell = 60$.

Fig. 5. Examples of center-of-mass kinetic energy distributions showing the quasi-elastic and the relaxed components in the reaction Ag + ^{14}N at various energies. (20)

Fig. 6. Contour plot of the center-of-mass cross section in the E, θ plane for Z = 19 in the reaction Au + ^{40}Ar at 288 MeV.(23)

Fig. 7. Average center-of-mass kinetic energies and widths of the distributions as a function of the Z of the fragment for the reaction Au + ^{86}Kr at 620 MeV.(24) The kinetic energies expected from the Coulomb repulsion of two spherical fragments is also shown.

Fig. 8. Laboratory cross sections as a function of Z for the relaxed component in the reaction Ag + ^{14}N.(20)

Fig. 9. Same as in Fig. 8 for the reaction Ag + ^{20}Ne. (22)

Fig. 10. Same as in Fig. 8 for the reaction Ag + ^{40}Ar. (21)

Fig. 11. Same as in Fig. 8 for the reaction Au + ^{40}Ar. (23)

Fig. 12. Same as in Fig. 8 for the reaction Ag + ^{84}Kr. (31)

Fig. 13. Same as in Fig. 8 for the reaction Au + ^{86}Kr. (24)

Fig. 14. Same as in Fig. 8 for the reaction Ta + ^{86}Kr. (32)

Fig. 15. Center-of-mass charge distributions for various kinetic energy bins at various lab angles in the reaction ^{197}Au + ^{86}Kr at 620 MeV. The energy bins for each Z start 50 MeV below the Coulomb barrier of two touching spheres and increase in steps of 25 MeV. The highest numbers correspond to the lowest kinetic energies.

Fig. 16. Center-of-mass angular distributions for the reaction Ag + ^{14}N. (20)

Fig. 17. Same as in Fig. 16 for the reaction Ag + ^{20}Ne. (22)

Fig. 18. Same as in Fig. 16 for the reaction Ag + ^{40}Ar. (21)

Fig. 19. Same as in Fig. 16 for the reaction Au + ^{40}Ar. (23)

Fig. 20. Same as in Fig. 16 for the reaction Ag + ^{84}Kr. (31)

Fig. 21. Same as in Fig. 16 for the reaction Au + ^{86}Kr. (24)

Fig. 22. Same as in Fig. 16 for the reaction Ta + ^{86}Kr. (32)

Fig. 23. Examples of contour plots of the center-of-mass cross section in the E, θ plane for various Z's in the reaction Au + ^{86}Kr. (24)

Fig. 24. Comparison between theoretical and experimental center-of-mass angular distributions for the reaction Ag + ^{40}Ar at 288 MeV. (14)

Fig. 25. Theoretical center-of-mass angular distributions for the reaction Ag + ^{40}Ar at 288 MeV. (14)

Fig. 26. Theoretical center-of-mass angular distributions for the reaction Au + ^{86}Kr at 620 MeV.

REFERENCES

1) L. G. Moretto, D. Heunemamn, R. C. Jared, R. C. Gatti and S. G. Thompson, Third Symposium on the Physics and Chemistry of Fission, August 1973, Rochester, N.Y. U.S.A, IAEA-SM-174/75.

2) A. G. Artukh, G. F. Gridnev, V. L. Mikheev, V. V. Volkov and J. Wilczynski, Nucl. Phys., A215 (1973) 91.

3) F. Hanappe, M. Lefort, C. Ngo, J. Peter, and B. Tamain, Phys. Rev. Lett., 32 (1974) 738.

4) K. L. Wolf, J. P. Unik, J. R. Huizenga, J. Birkelund, H. Freiesleben V. E. Viola, Phys. Rev. Lett., 33 (1974) 1105.

5) D. Glas and U. Mosel, Phys. Lett., 49B (1974) 301.

6) R. A. Broglia, C. H. Dasso and A. Winther, Phys. Lett., 53B (1974) 301.

7) D. H. E. Gross and H. Kalinowski, Phys. Lett., 48B (1974) 302.

8) D. H. E. Gross, Nucl. Phys., A240 (1975) 472.

9) C. F. Tsang, Physica Scripta, 10A (1974) 90.

10) R. Bass, Nucl. Phys., A231 (1974) 45.

11) J. R. Nix and A. J. Sierk, Physica Scripta, 10A (1974).

12) J. P. Bondorf, M. I. Sobel and D. Sperber, Phys. Reports, 15C (1974) 83.

13) J. P. Bondorf, J. R. Huizenga, M. Sobel and D. Sperber, Phys. Rev., 11C (1975) 1265.

14) L. G. Moretto and J. S. Sventek, Phys. Lett., 58B (1975) 26.

15) V. V. Volkov, Proc. of the Int. Conf. on Reactions between Complex Nuclei, Nashville (1974), eds. R. L. Robinson et al. Vol. 2 (1974) 363, Amsterdam, North Holland.

16) B. Gatty, D. Guerreau, M. Lefort, J. Pouthas, X. Tarrago, J. Galin, B. Cauvin, J. Girard and H. Nifenecker, J. de Phys., 35 (1974) L117; Z. Phys., A273 (1975) 65.

17) B. Gatty, D. Guerreau, M. Lefort, X. Tarrago, J. Galin, B. Cauvin, J. Girard and H. Nifenecker, Nucl. Phys., A253 (1975) 511.

18) S. G. Thompson, L. G. Moretto, R. C. Jared, R. P. Babinet, J. Galin, M. M. Fowler, R. C. Gatti and J. B. Hunter, Physica Scripta, 10A (1974).

19. L. G. Moretto, R. P. Babinet, J. Galin, and S. G. Thompson, Phys. Lett., 58B (1975) 31.

20) L. G. Moretto, S. K. Kataria, R. C. Jared, R. Schmitt and S. G. Thompson, Nucl. Phys., A255 (1975) 491.

21) J. Galin, L. G. Moretto, R. Babinet, R. Schmitt, R. Jared and S. G. Thompson, Nucl. Phys., A255 (1975) 472.

22. R. Babinet, L. G. Moretto, J. Galin, R. Jared, J. Moulton and S. G. Thompson, Nucl. Phys., A258 (1976) 172.

23) L. G. Moretto, J. Galin, R. Babinet, Z. Fraenkel, R. Schmitt, R. Jared and S. G. Thompson, Lawrence Berkeley Laboratory Report No. LBL-4084 (1975) to be published in Nuclear Physics A.

24) L. G. Moretto, B. Cauvin, P. Glässel, R. Jared, P. Russo, J. Sventek and G. Wozniak, Lawrence Berkeley Laboratory Report No. LBL-4362, (1976), to be published in Physical Review Letters.

25) W. Nörenberg, Phys. Lett., 53B (1974) 289.

26) C. Ngo, J. Peter, B. Tamain, M. Berlanger and F. Hanappe, preprint IPNO-RC-75-09.

27) J. Randrup, W. J. Swiatecki and C. F. Tsang, Lawrence Berkeley Laboratory Report No. LBL-3603 (1974).

28) C. Ngo, B. Tamain, J. Galin, M. Beiner and R. J. Lombard, Nucl. Phys., A240 (1975) 353.

29) J. Wilczynski, Phys. Lett., 47B (1973) 484.

30) M. Lefort, C. Ngo, J. Peter and B. Tamain, Nucl. Phys., A197 (1972) 485.

31) R. P. Schmitt, P. Russo, R. Babinet, R. Jared and L. G. Moretto, to be published.

32) P. Russo, P. Glassel, B. Cauvin, G. Wozniak, R. P. Schmitt, R. Jared and L. G. Moretto, to be published.

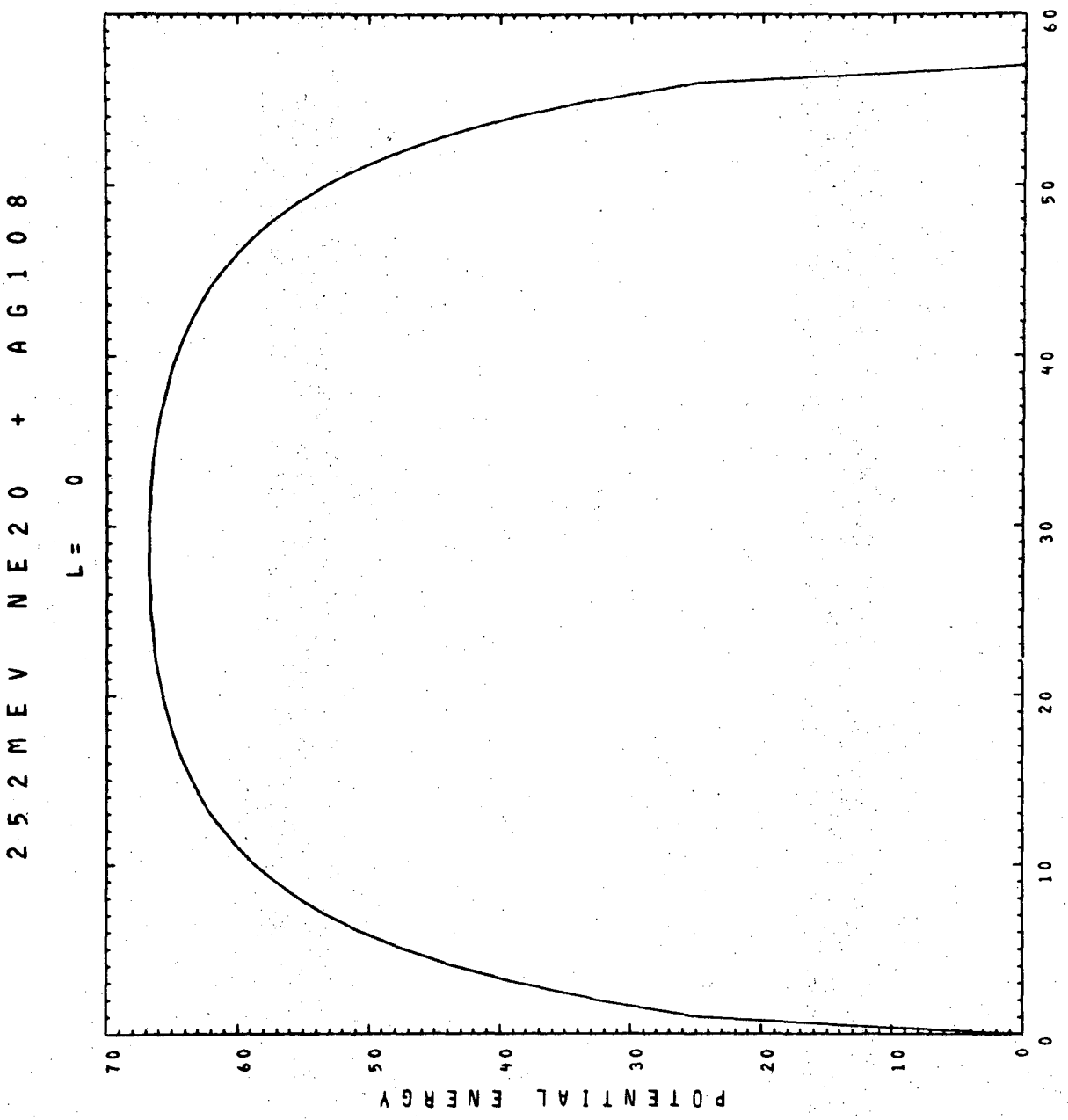

Fig.1a

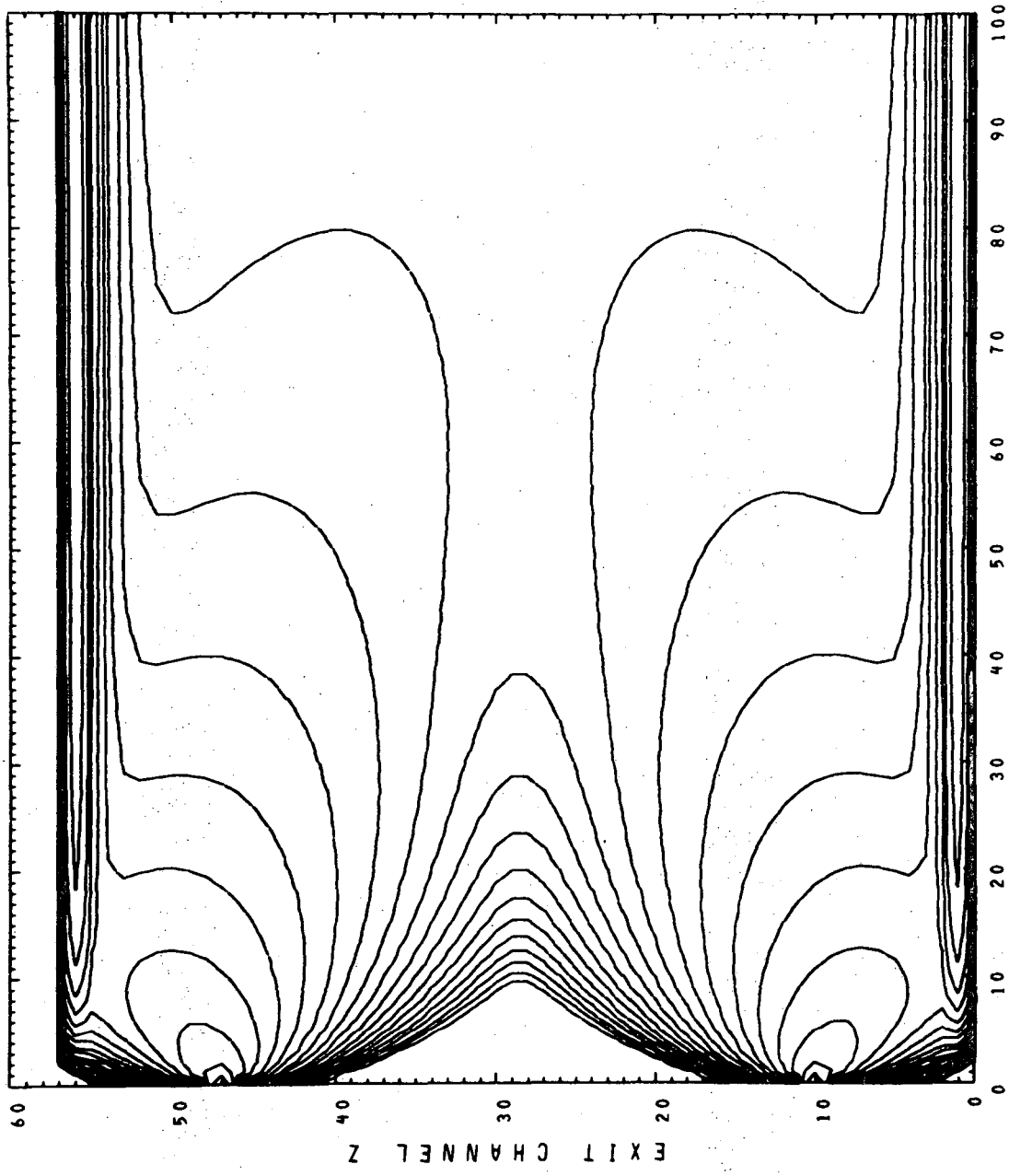
252MEV NE20 + AG108
L= 0 , KAPPA= .5000E+21 [(SEC*FM**2)**-1]
EXIT CHANNEL Z
TIME(IN UNITS OF 10**(-22) SECONDS)
0
10
20
30
40
50
60
70
80
90
100

Fig. 1b

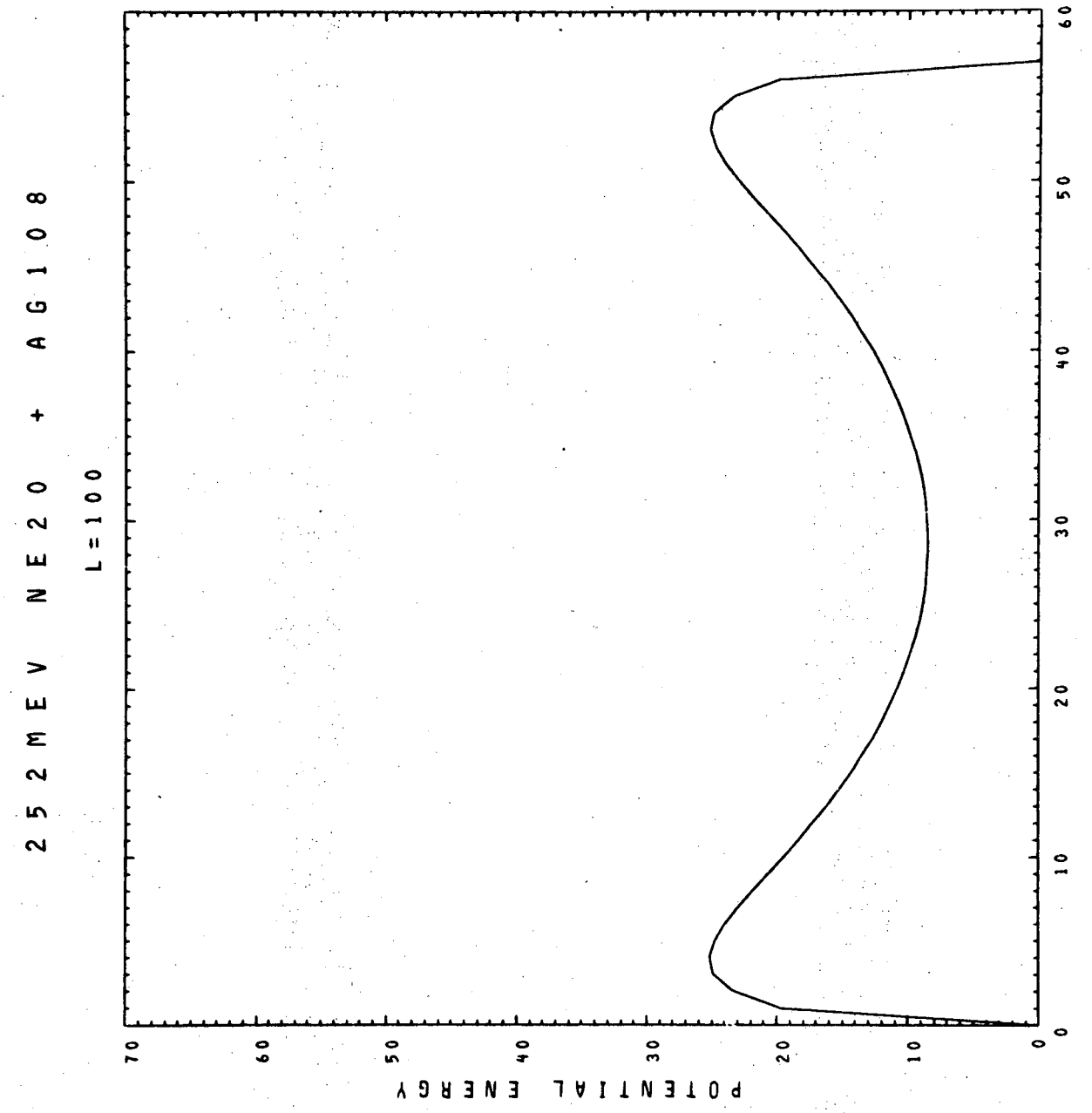

Fig. 2a

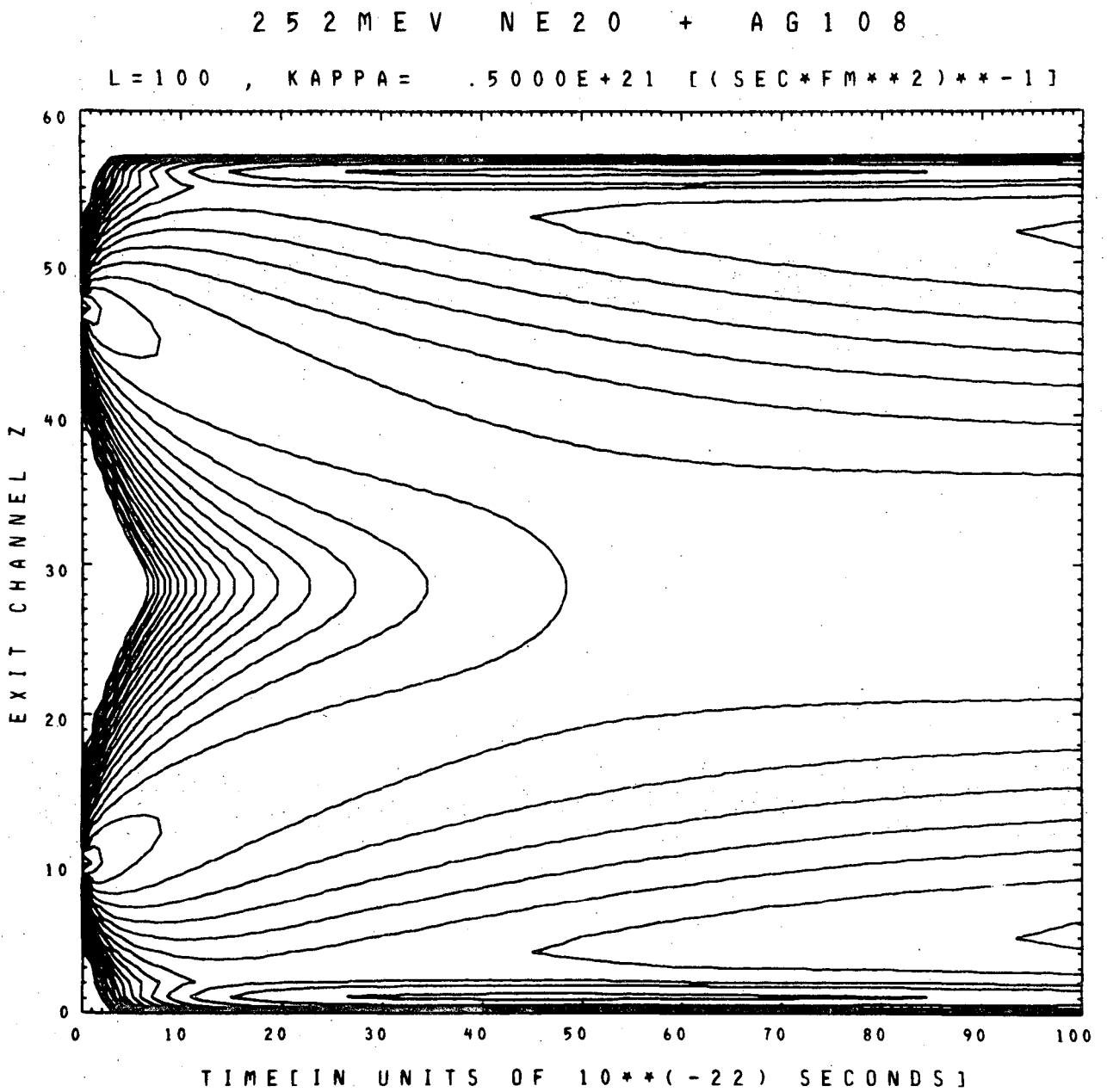
252 MEV NE20 + AG108
L=100 , KAPPA= .5000E+21 [(SEC*FM**2)**-1]
EXIT CHANNEL Z
0
10
20
30
40
50
60
0
10
20
30
40
50
60
70
80
90
100
TIME[IN UNITS OF 10**(-22) SECONDS]

Fig. 2b

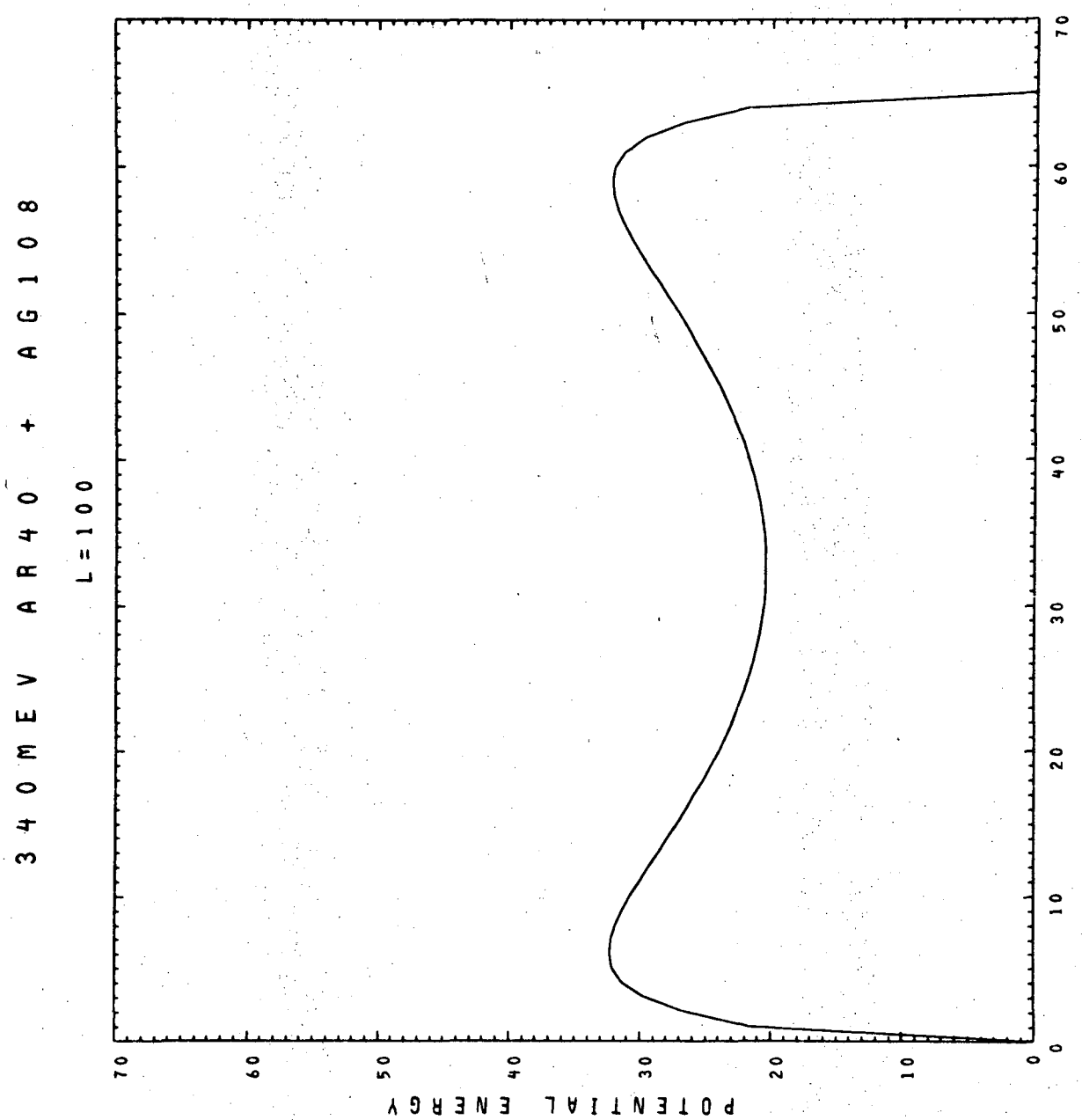

Fig. 3a

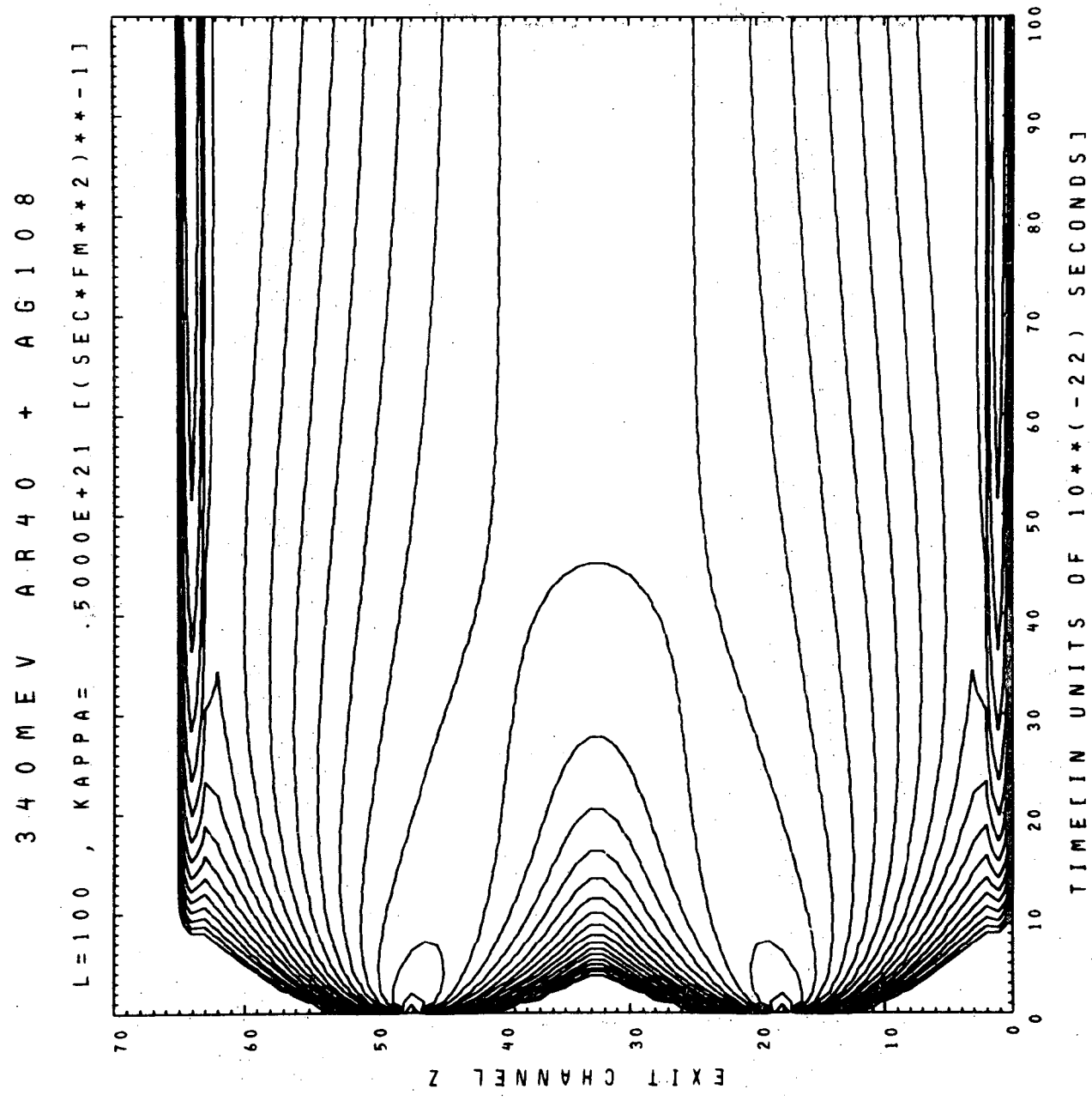
340MEV AR40 + AG108
L=100 , KAPPA= .5000E+21 [(SEC*FM**2)**-1]
EXIT CHANNEL Z
TIME IN UNITS OF 10**(-22) SECONDS
0
10
20
30
40
50
60
70
80
90
100

Fig. 3b

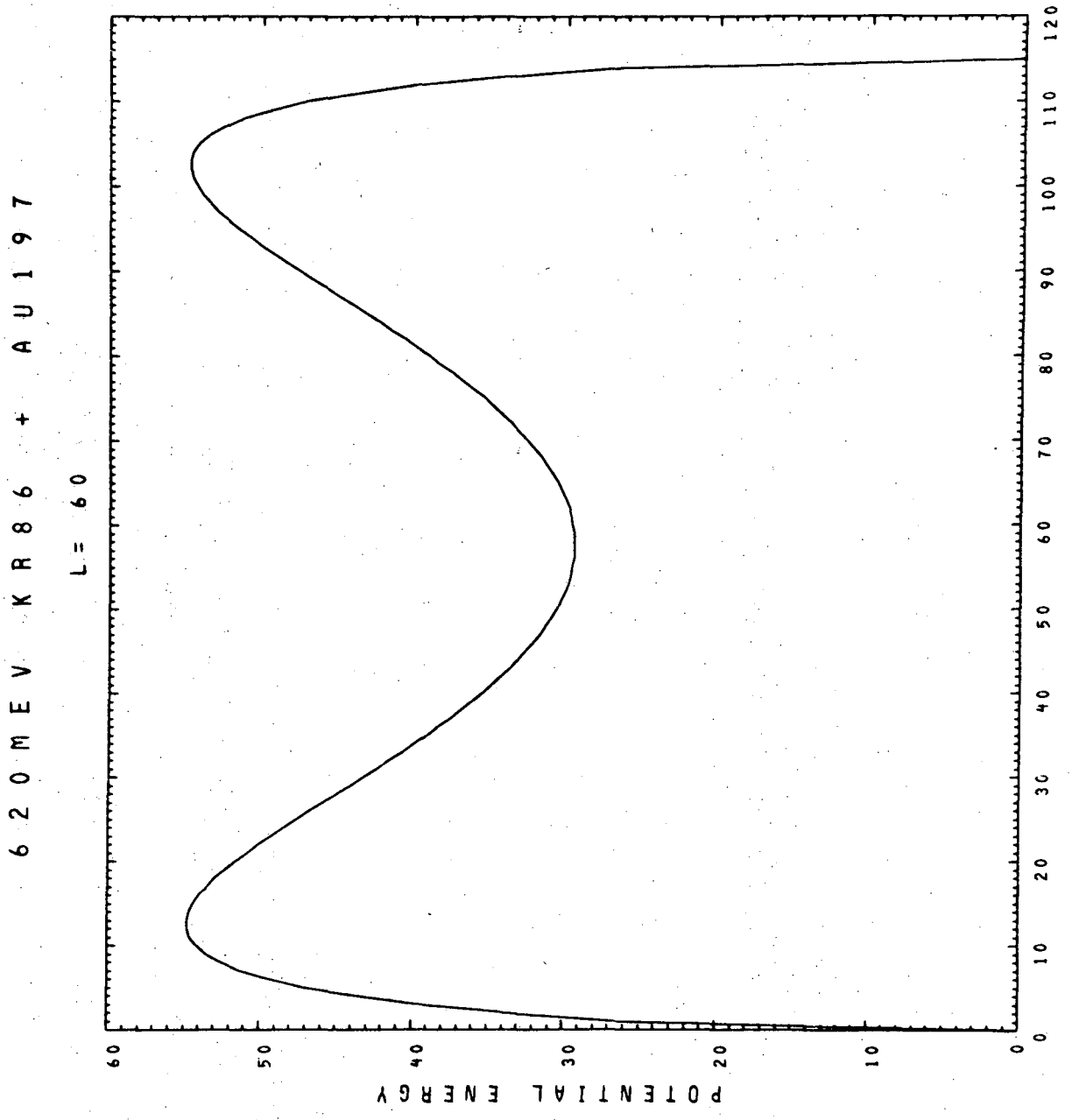

Fig. 4a

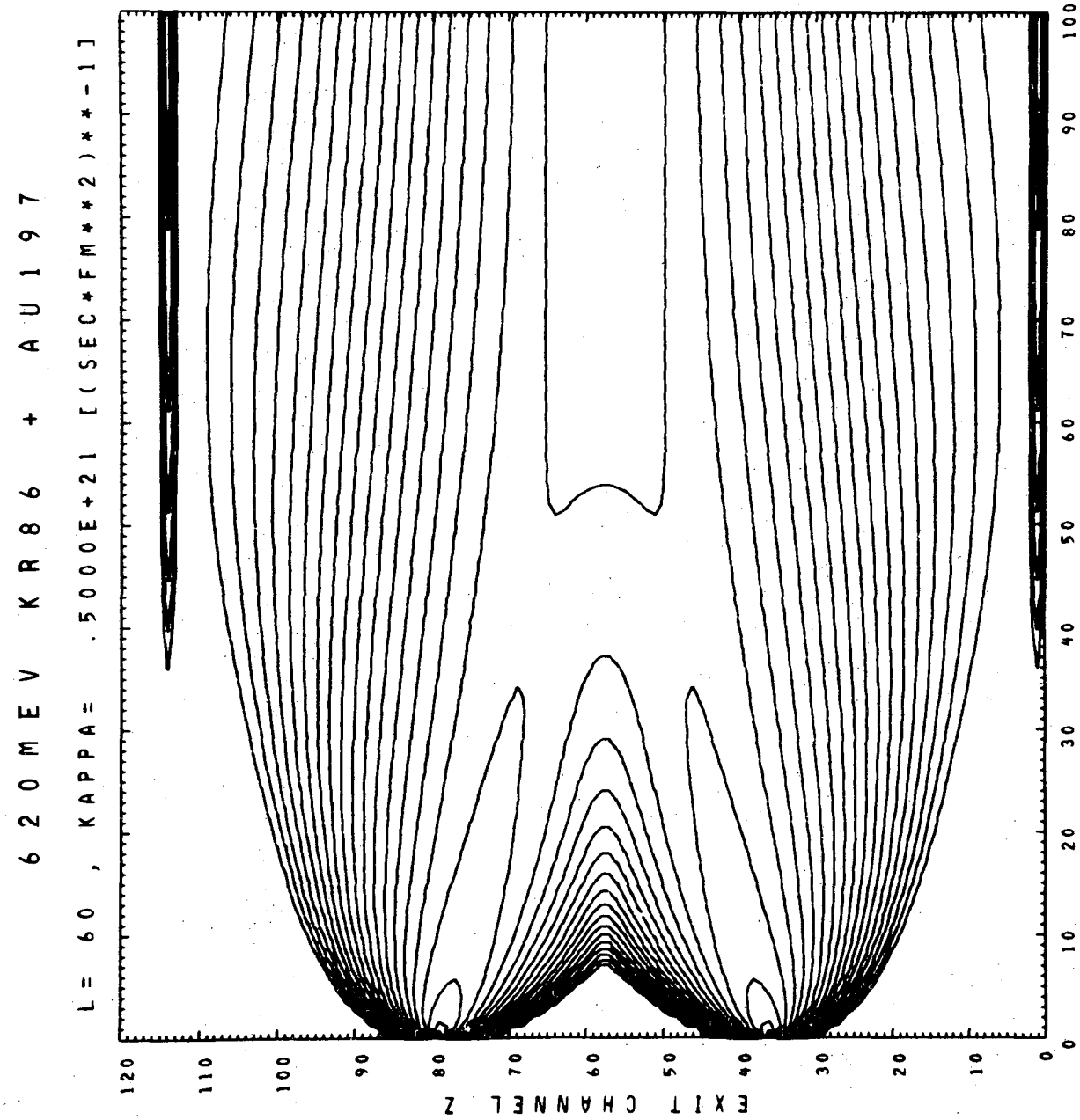
620MEV KR86 + AU197
L= 60 , KAPPA= .5000E+21 [(SEC*FM**2)**-1]
EXIT CHANNEL Z
TIME[IN UNITS OF 10**(-22) SECONDS]
0
10
20
30
40
50
60
70
80
90
100
110
120

Fig. 4b

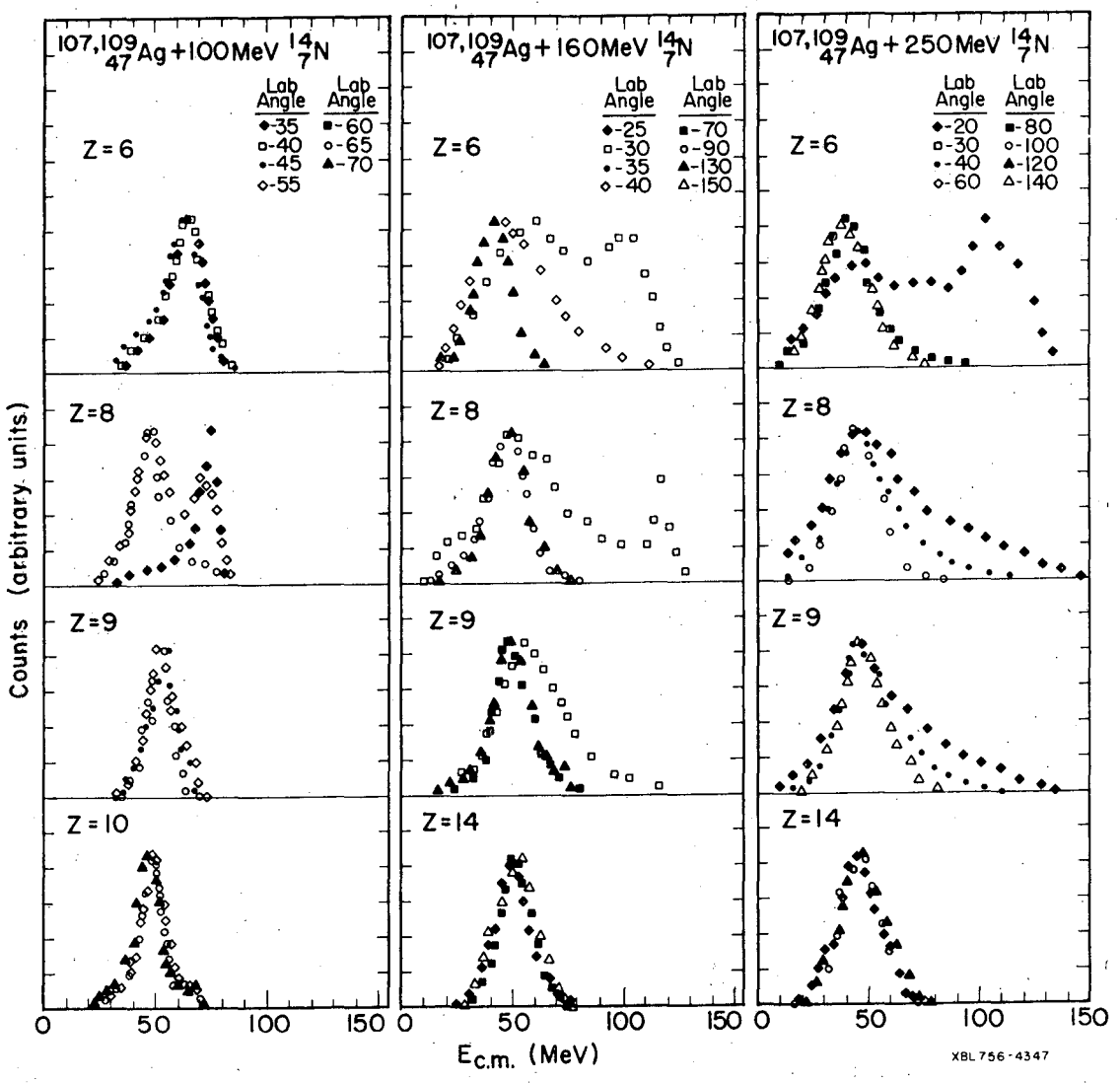

Fig. 5

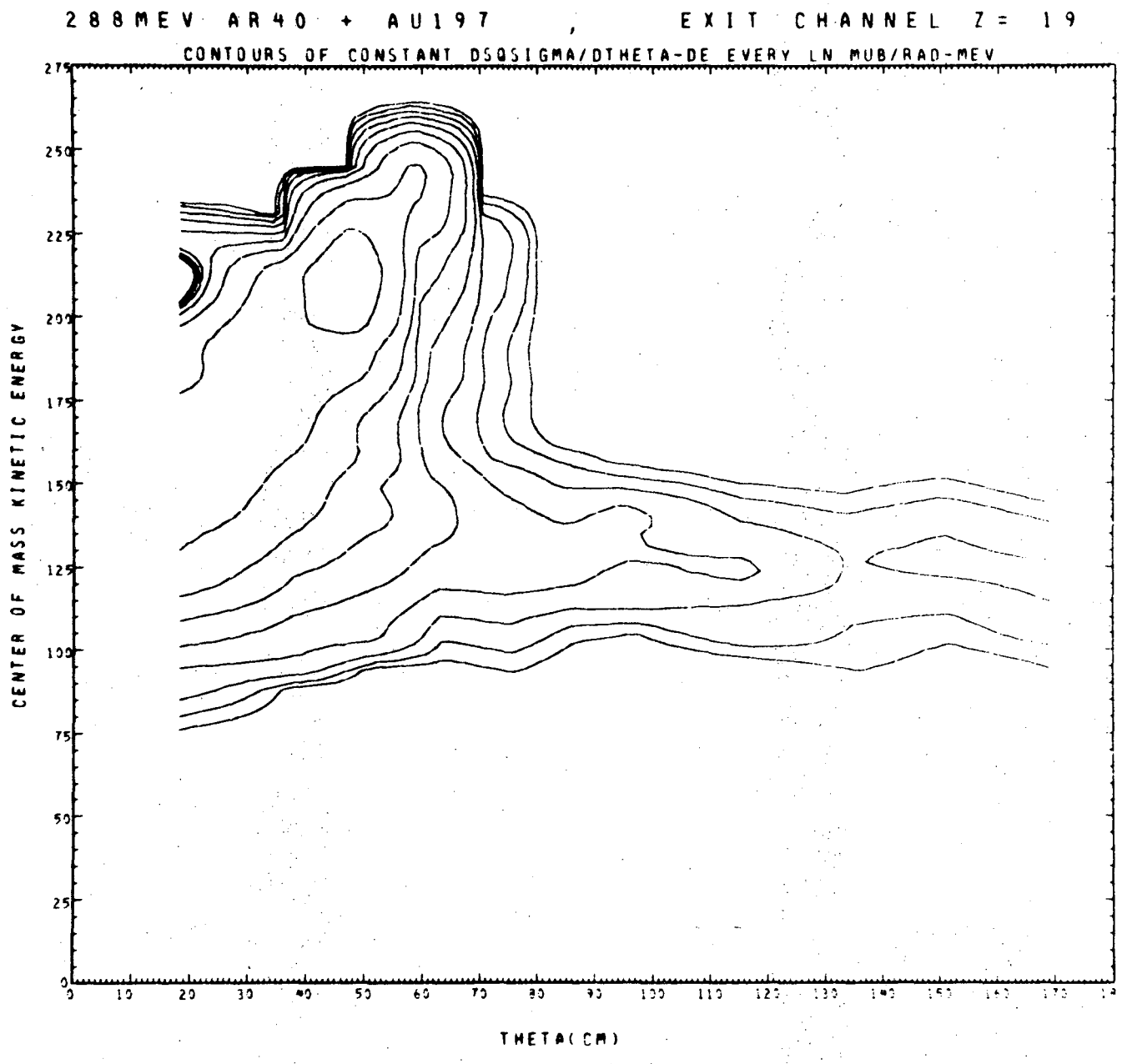
288MEV AR40 + AU197 , EXIT CHANNEL Z = 19
CONTOURS OF CONSTANT DSQSIGMA/DTHETA-DE EVERY LN MUB/RAD-MEV
CENTER OF MASS KINETIC ENERGY
THETA(CM)
0
25
50
75
100
125
150
175
200
225
250
275
0
10
20
30
40
50
60
70
80
90
100
110
120
130
140
150
160
170

Fig. 6

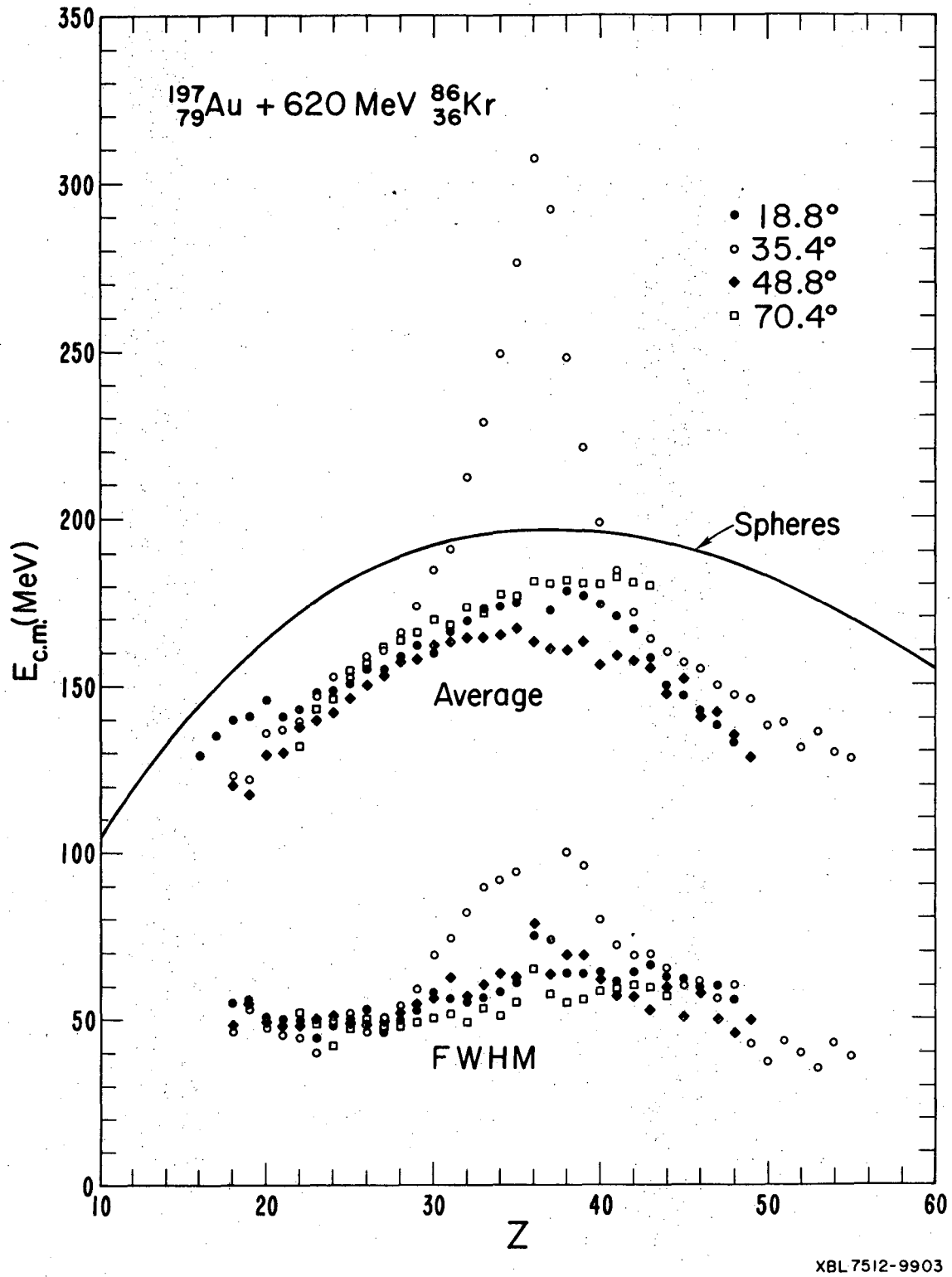

Fig. 7

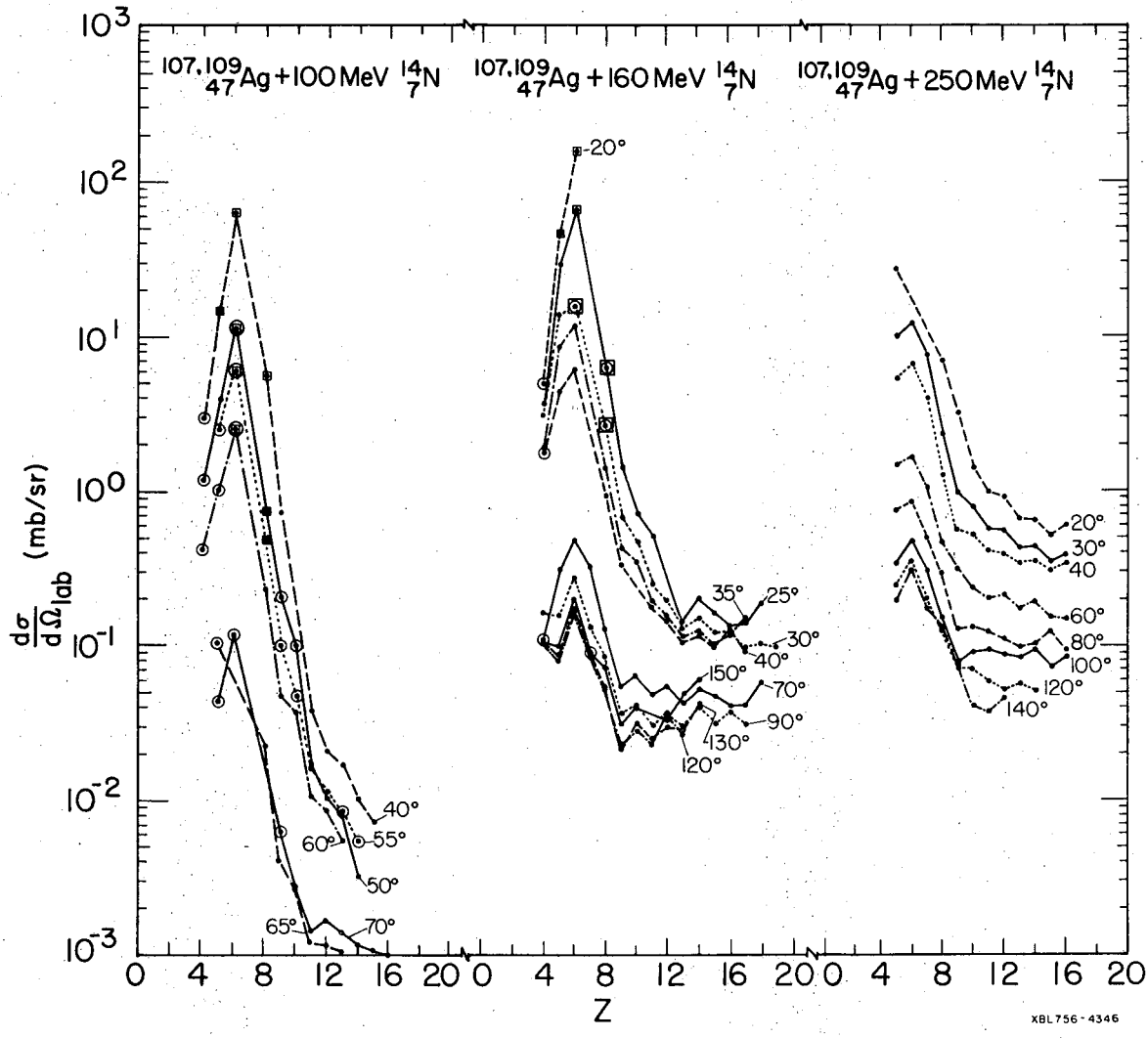
107,109 47Ag + 100 MeV 14 7N
107,109 47Ag + 160 MeV 14 7N
107,109 47Ag + 250 MeV 14 7N
dσ/dΩ lab (mb/sr)
Z
XBL756-4346
-20°
35°
25°
30°
40°
150°
70°
90°
130°
120°
40°
60°
55°
50°
65°
70°
20°
30°
40
60°
80°
100°
120°
140°

Fig. 8

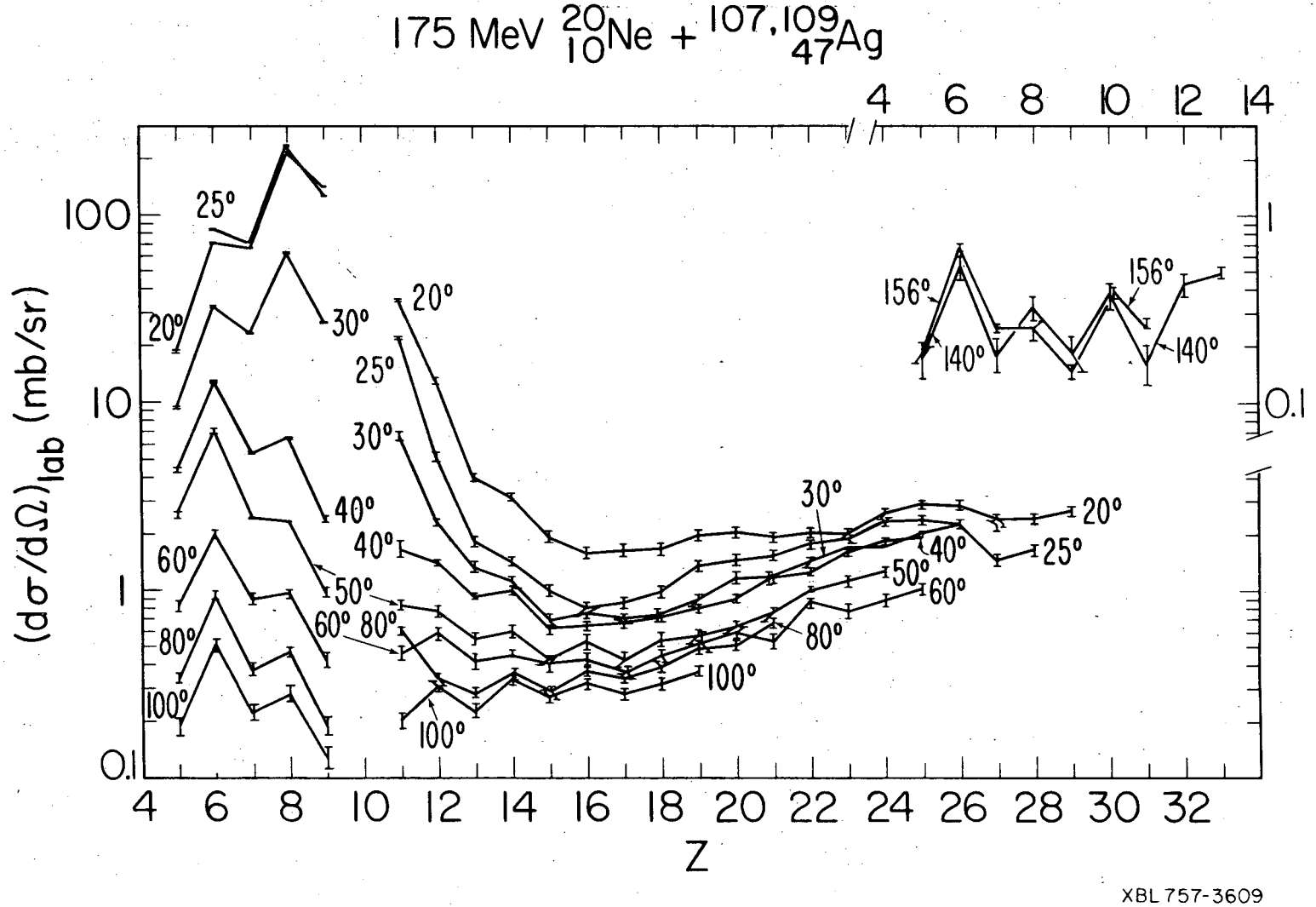

XBL 757-3609

Fig. 9

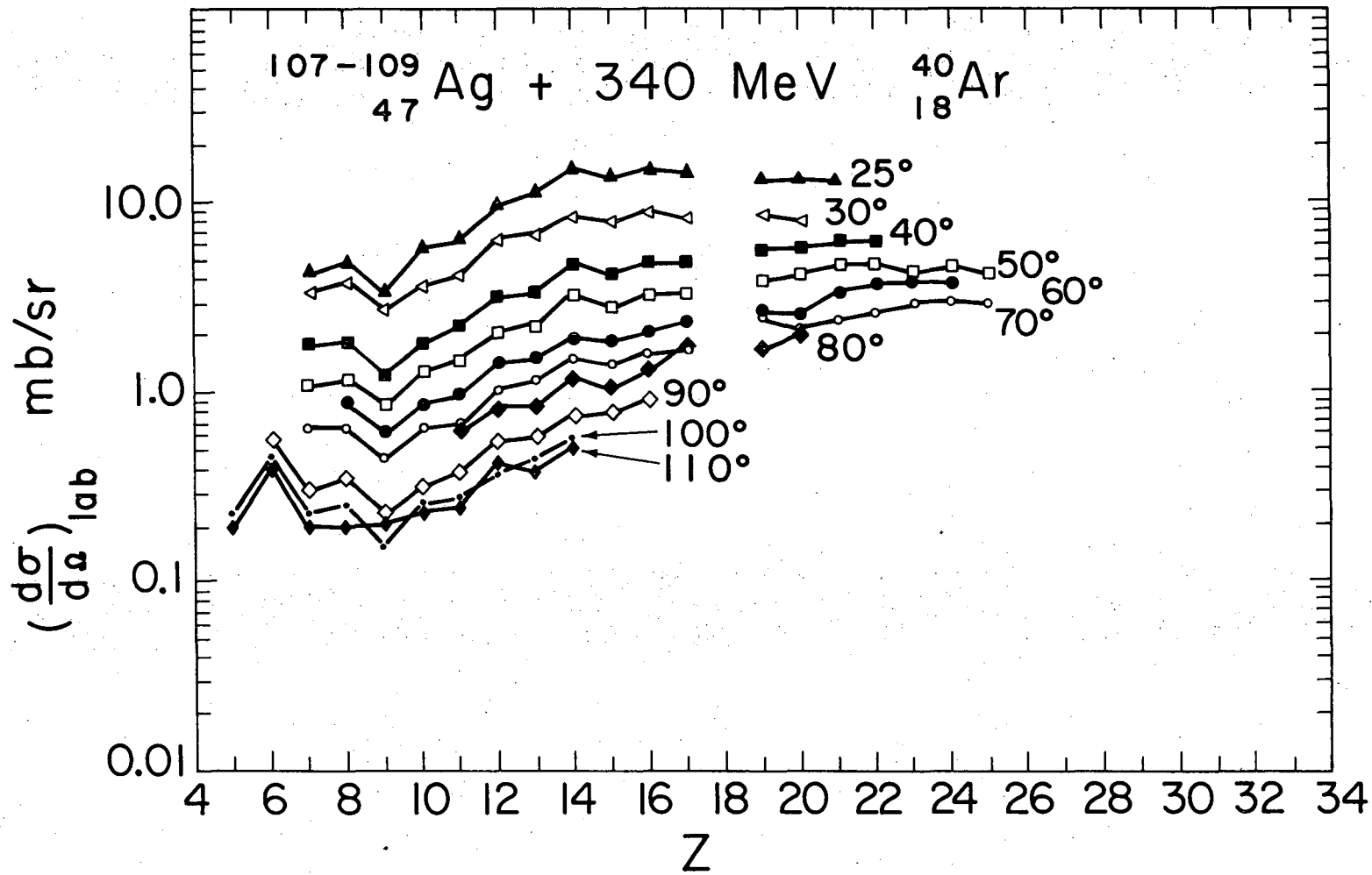
107-109 47 Ag + 340 MeV 40 18 Ar
25°
30°
40°
50°
60°
70°
80°
90°
100°
110°
10.0
1.0
0.1
0.01
(dσ/dΩ)lab mb/sr
4 6 8 10 12 14 16 18 20 22 24 26 28 30 32 34
Z
XBL752-2301

Fig. 10

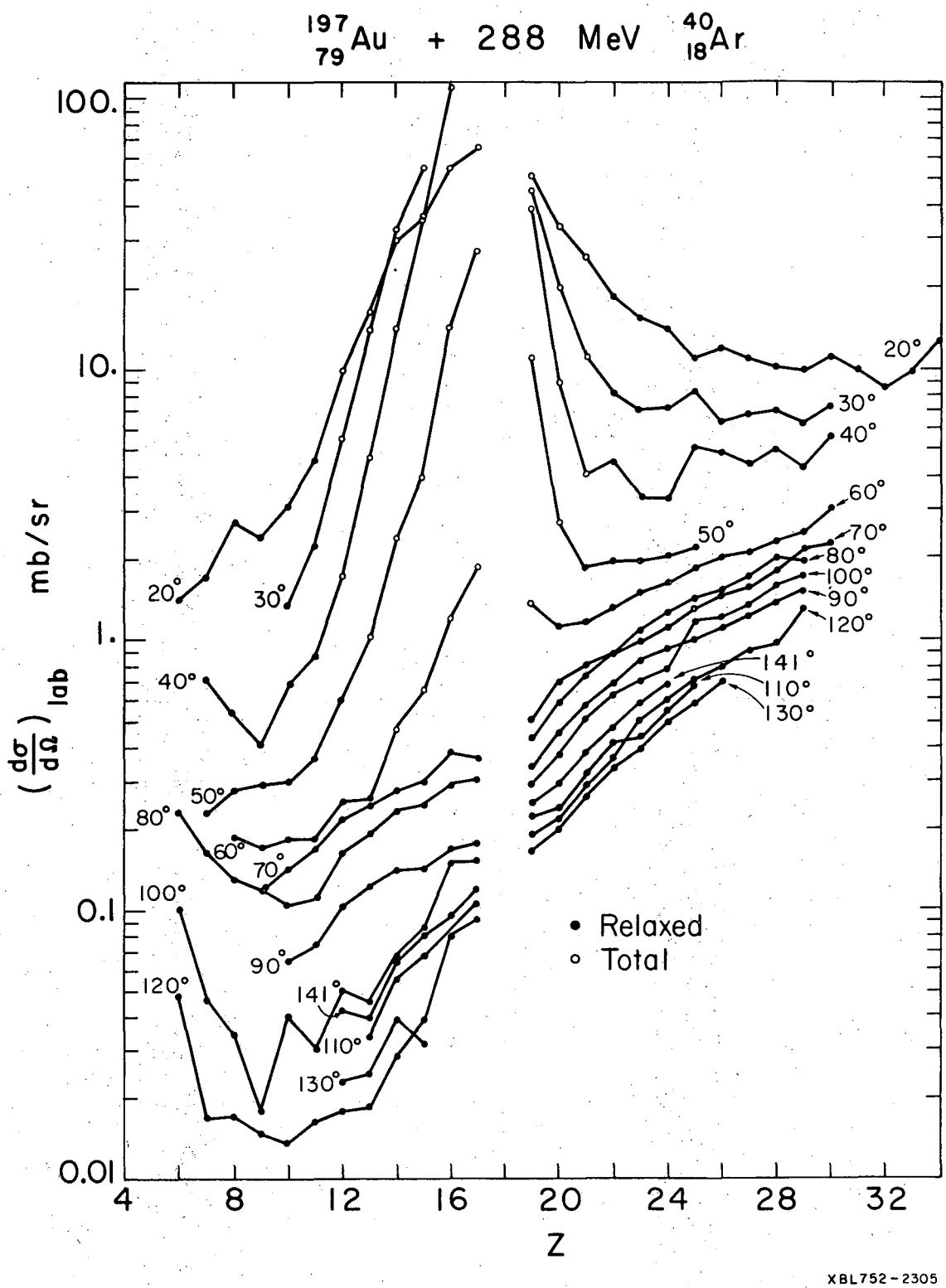

Fig. 11

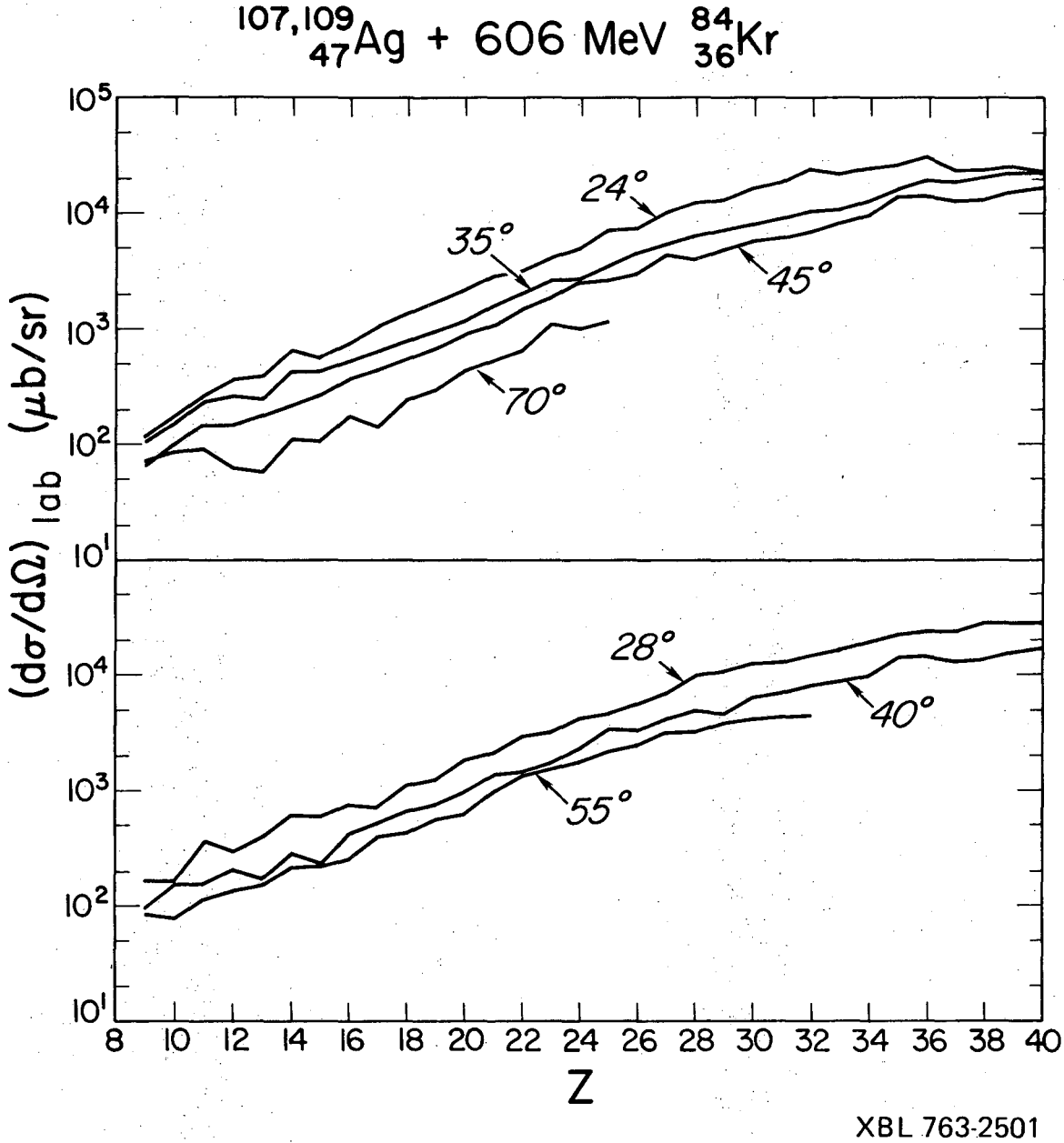
$^{107,109}_{47}$Ag + 606 MeV $^{84}_{36}$Kr
$(d\sigma/d\Omega)_{lab}$ (μb/sr)
10^5
10^4
10^3
10^2
10^1
24°
35°
45°
70°
28°
40°
55°
8 10 12 14 16 18 20 22 24 26 28 30 32 34 36 38 40
Z
XBL 763-2501

Fig. 12

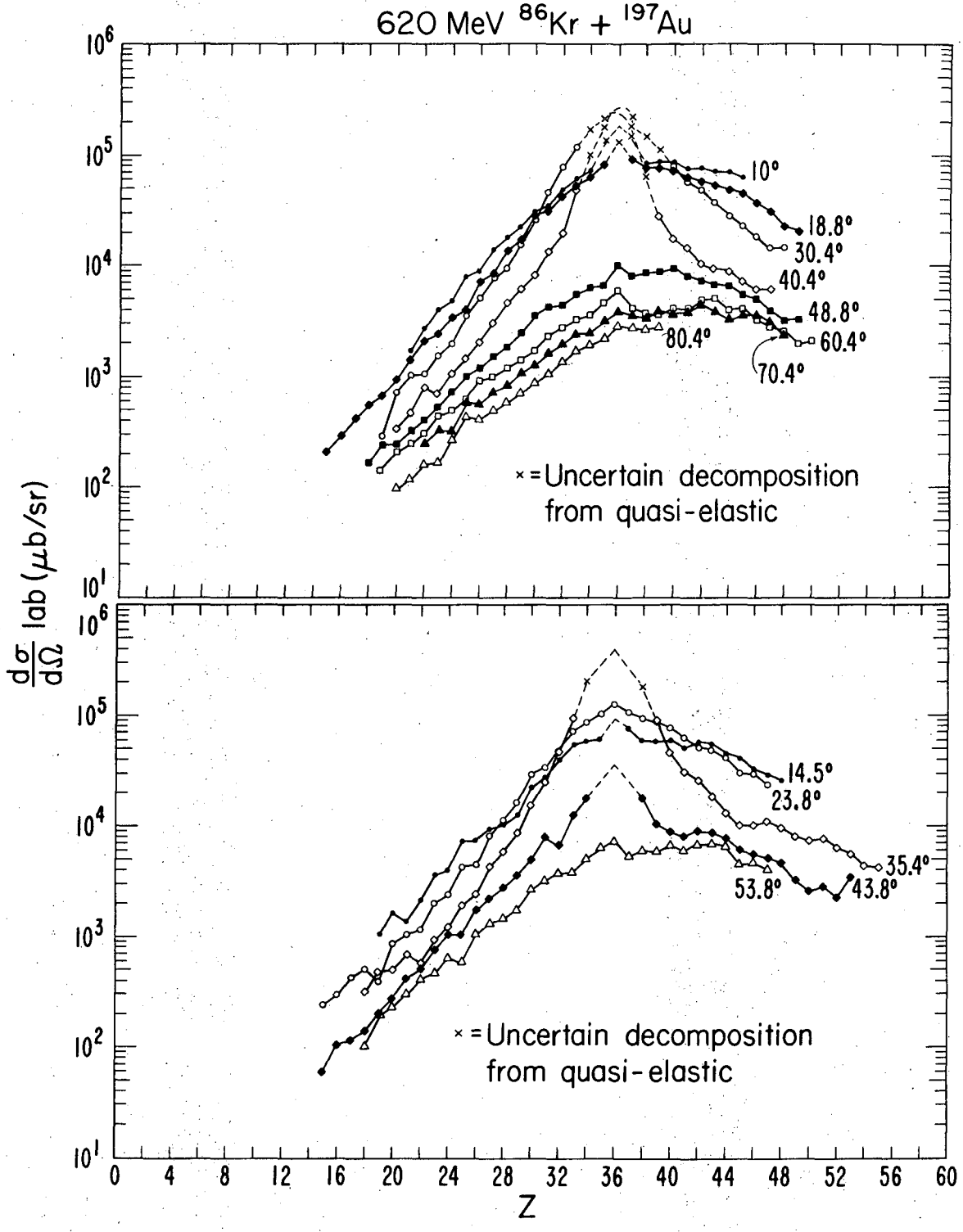

Fig. 13

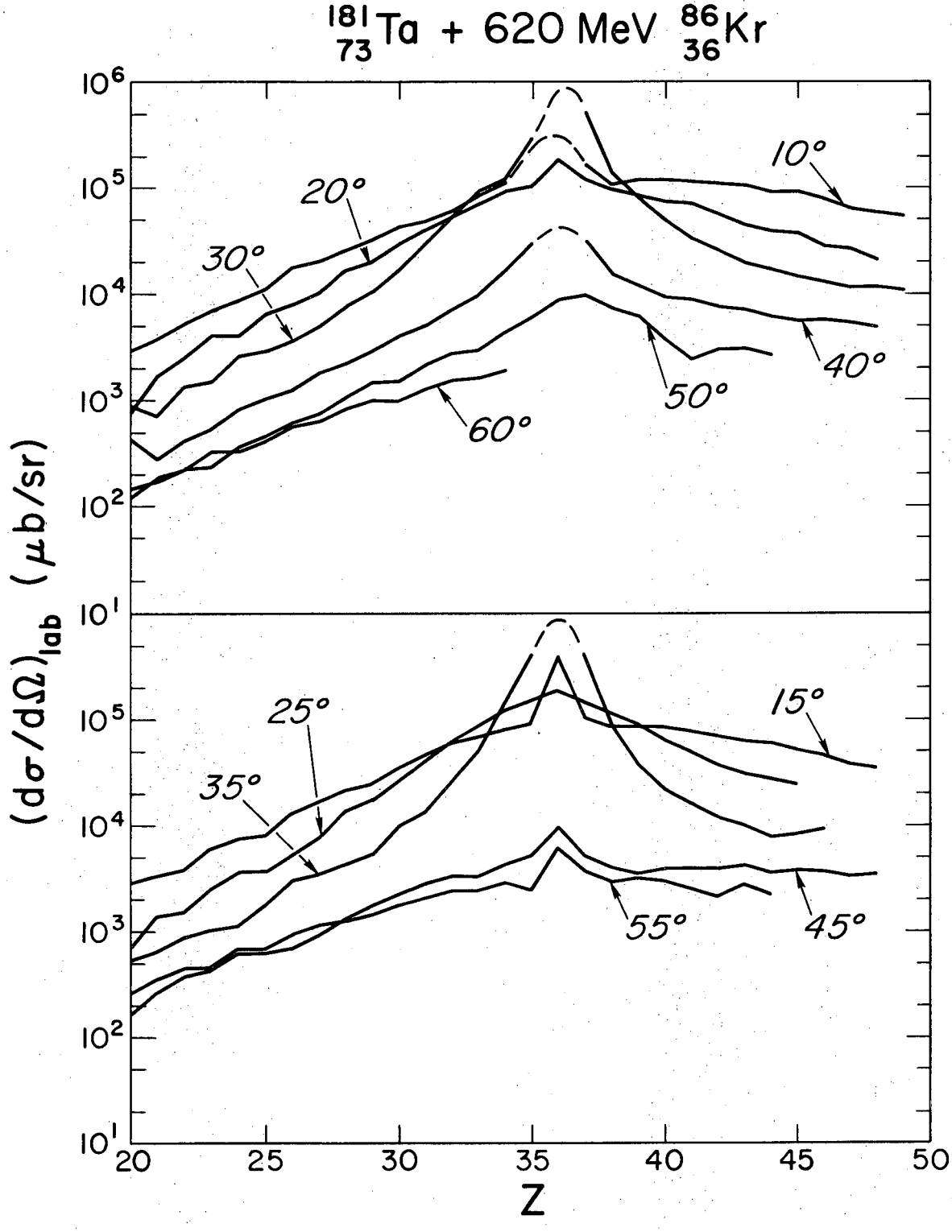
$^{181}_{73}$Ta + 620 MeV $^{86}_{36}$Kr
$(d\sigma/d\Omega)_{lab}$ (μb/sr)
Z
10°
15°
20°
25°
30°
35°
40°
45°
50°
55°
60°
XBL 763-2502

Fig. 14

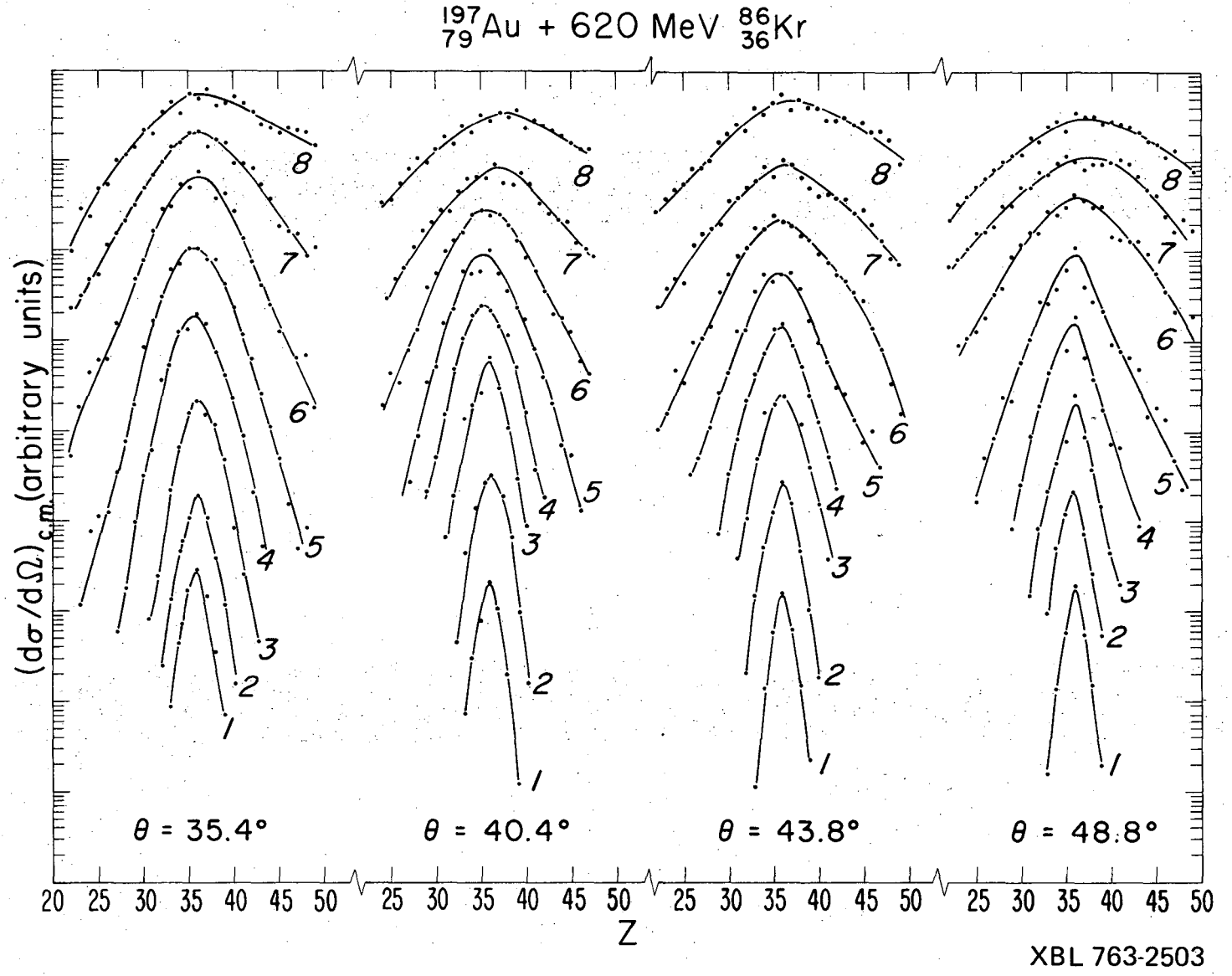

Fig. 15

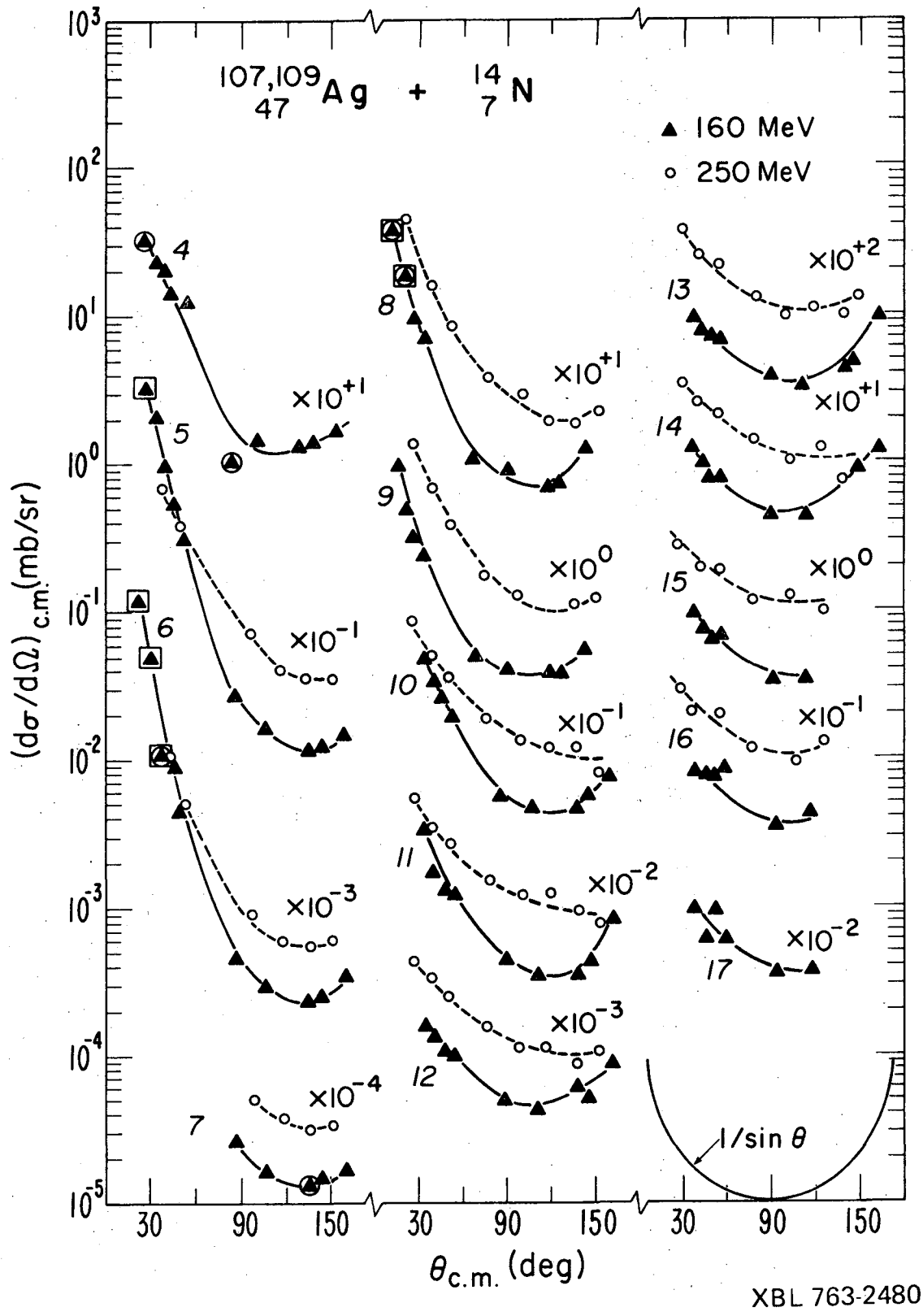
107,109 Ag + 14 N
47 7
160 MeV
250 MeV
(dσ/dΩ)c.m.(mb/sr)
θc.m. (deg)
1/sin θ
×10+2
×10+1
×10+1
×10+1
×10⁰
×10⁰
×10-1
×10-1
×10-1
×10-2
×10-2
×10-3
×10-3
×10-4
4
5
6
7
8
9
10
11
12
13
14
15
16
17
XBL 763-2480

Fig. 16

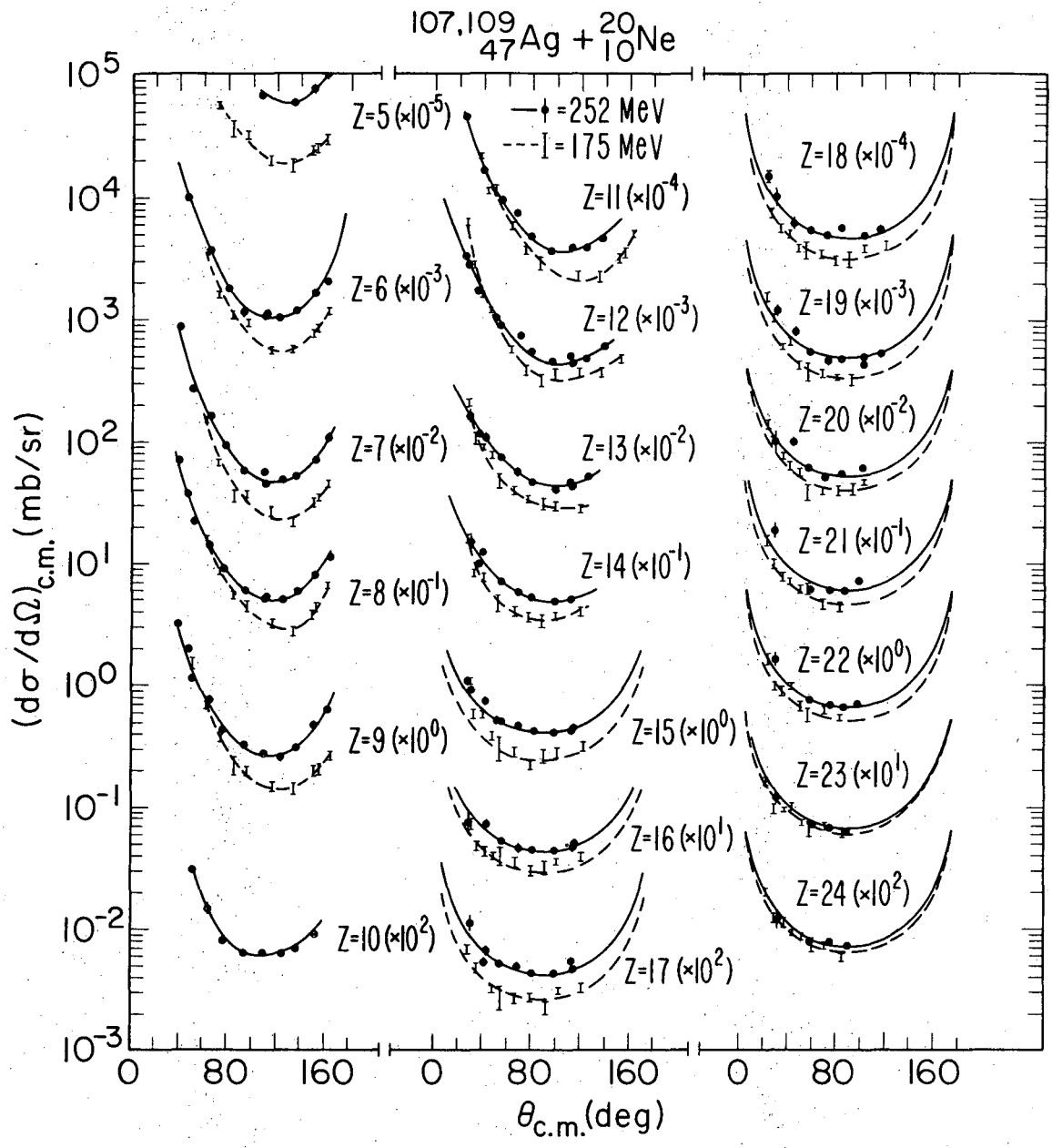

Fig. 17

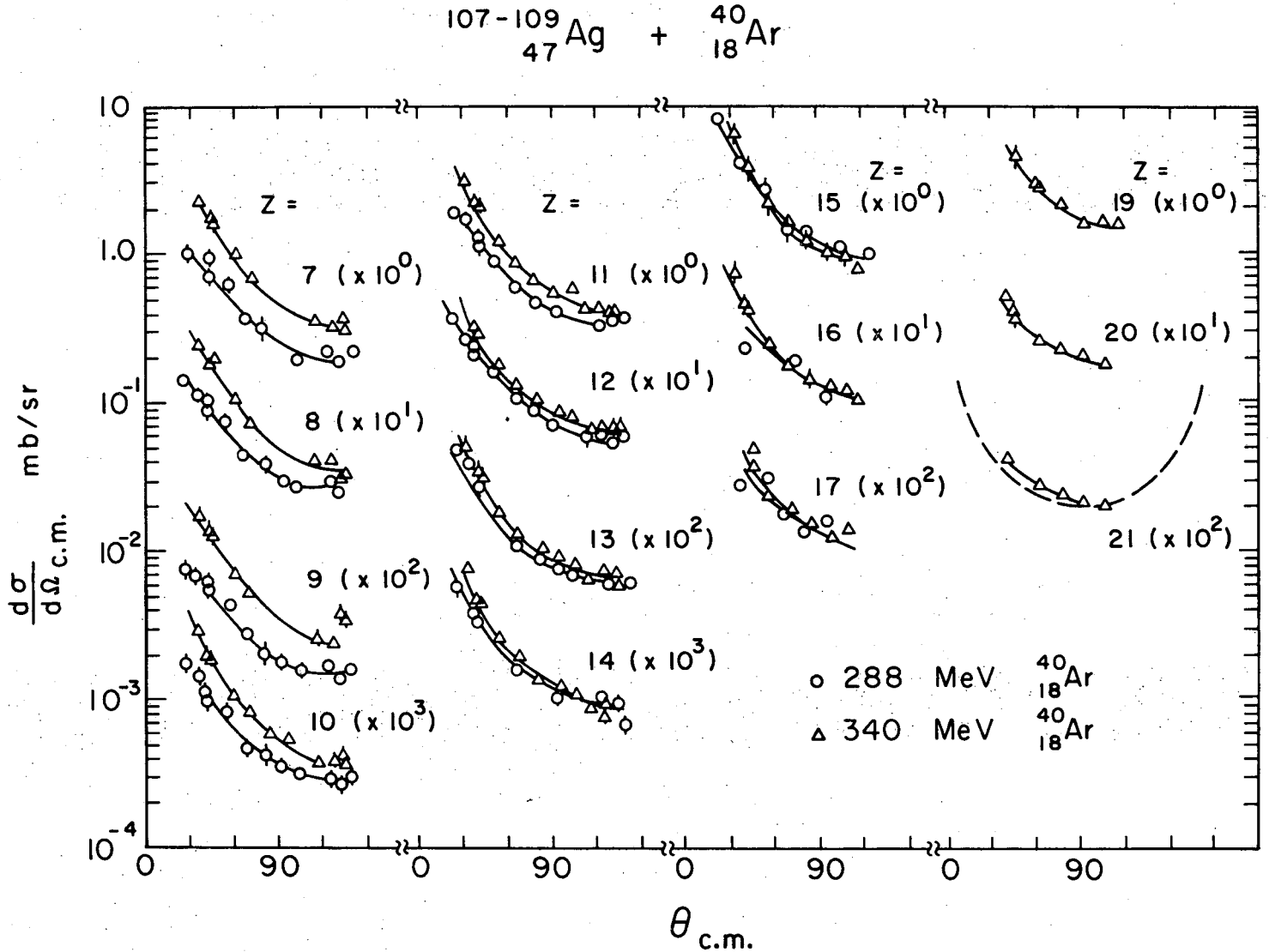

XBL752-2302

Fig. 18

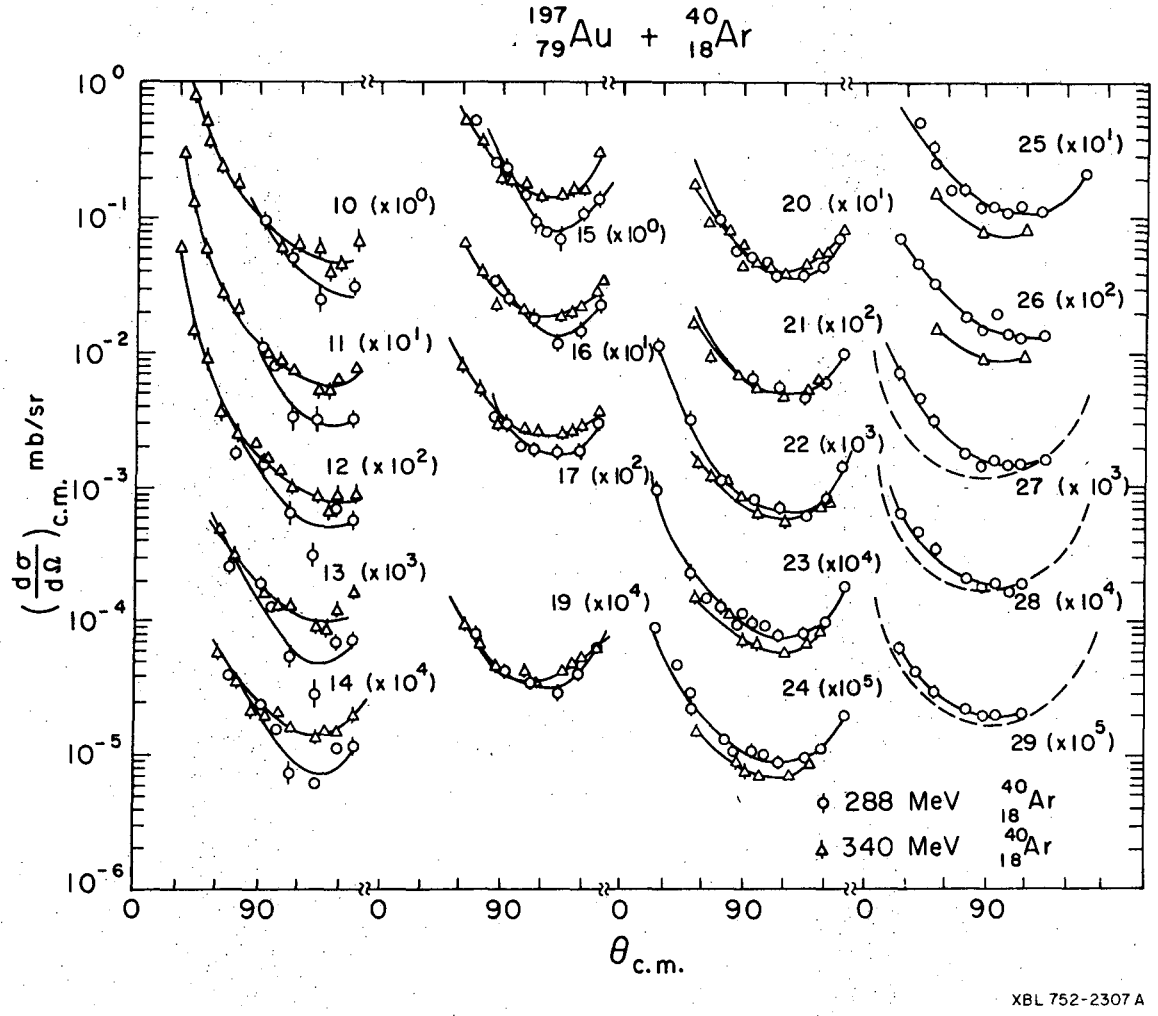

Fig. 19

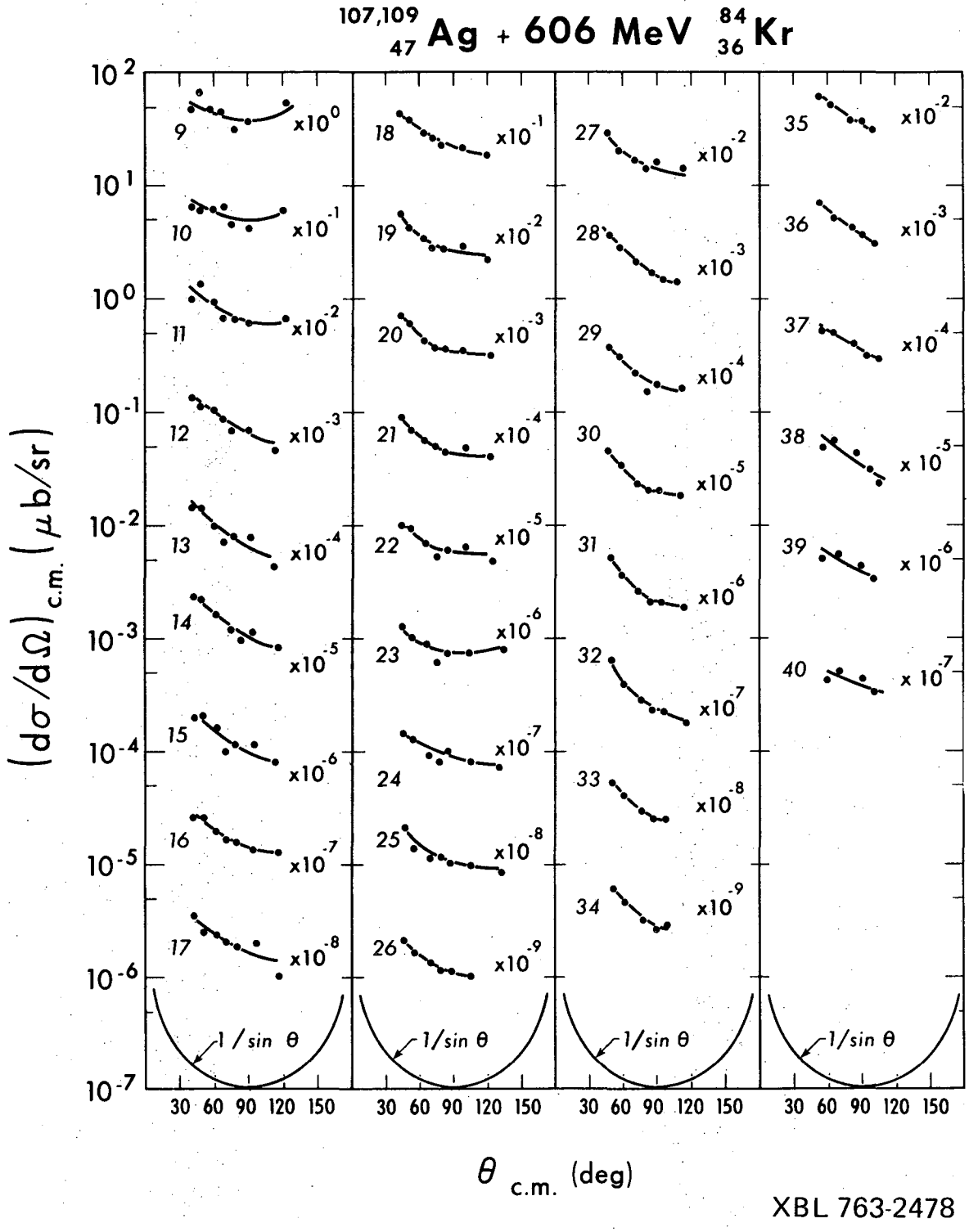
107,109 47 Ag + 606 MeV 84 36 Kr
(dσ/dΩ)c.m. (μb/sr)
θ c.m. (deg)
1/sin θ
30 60 90 120 150
XBL 763-2478

Fig. 20

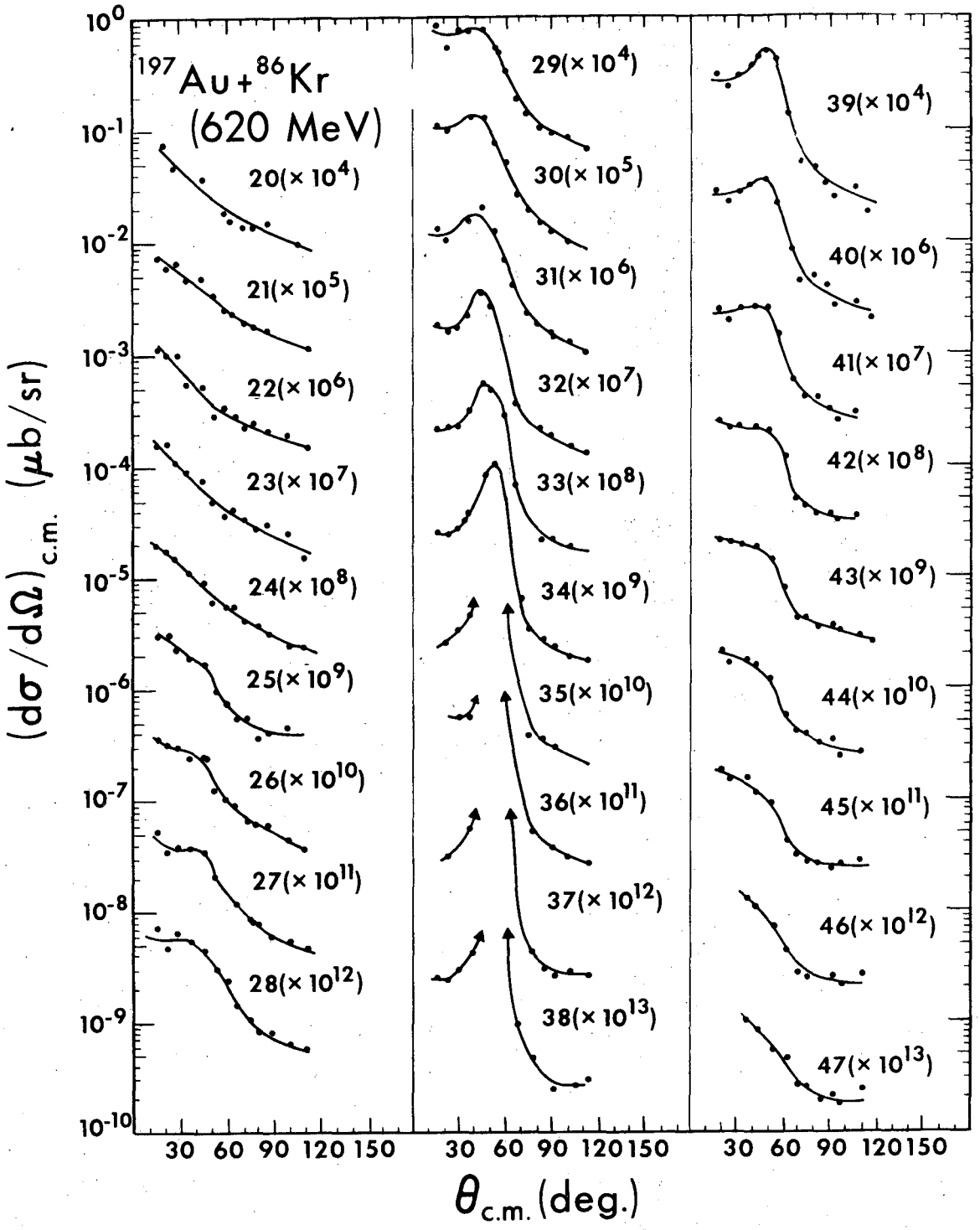

XBL 7512-9891

Fig.21

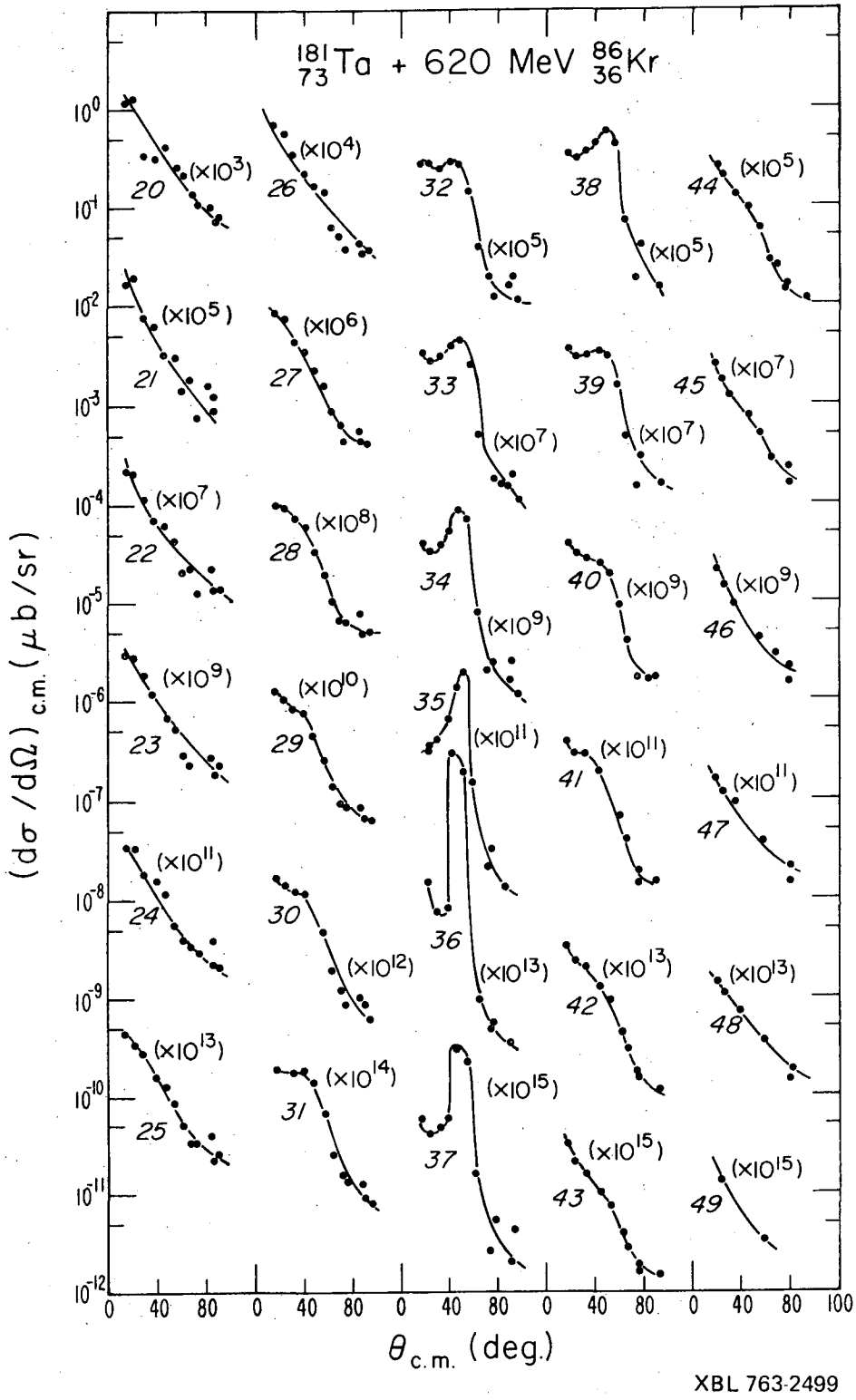
$^{181}_{73}$Ta + 620 MeV $^{86}_{36}$Kr
$(d\sigma/d\Omega)_{c.m.}$ (μb/sr)
$\theta_{c.m.}$ (deg.)
20 (×10³)
21 (×10⁵)
22 (×10⁷)
23 (×10⁹)
24 (×10¹¹)
25 (×10¹³)
26 (×10⁴)
27 (×10⁶)
28 (×10⁸)
29 (×10¹⁰)
30 (×10¹²)
31 (×10¹⁴)
32 (×10⁵)
33 (×10⁷)
34 (×10⁹)
35 (×10¹¹)
36 (×10¹³)
37 (×10¹⁵)
38 (×10⁵)
39 (×10⁷)
40 (×10⁹)
41 (×10¹¹)
42 (×10¹³)
43 (×10¹⁵)
44 (×10⁵)
45 (×10⁷)
46 (×10⁹)
47 (×10¹¹)
48 (×10¹³)
49 (×10¹⁵)
XBL 763-2499

Fig. 22

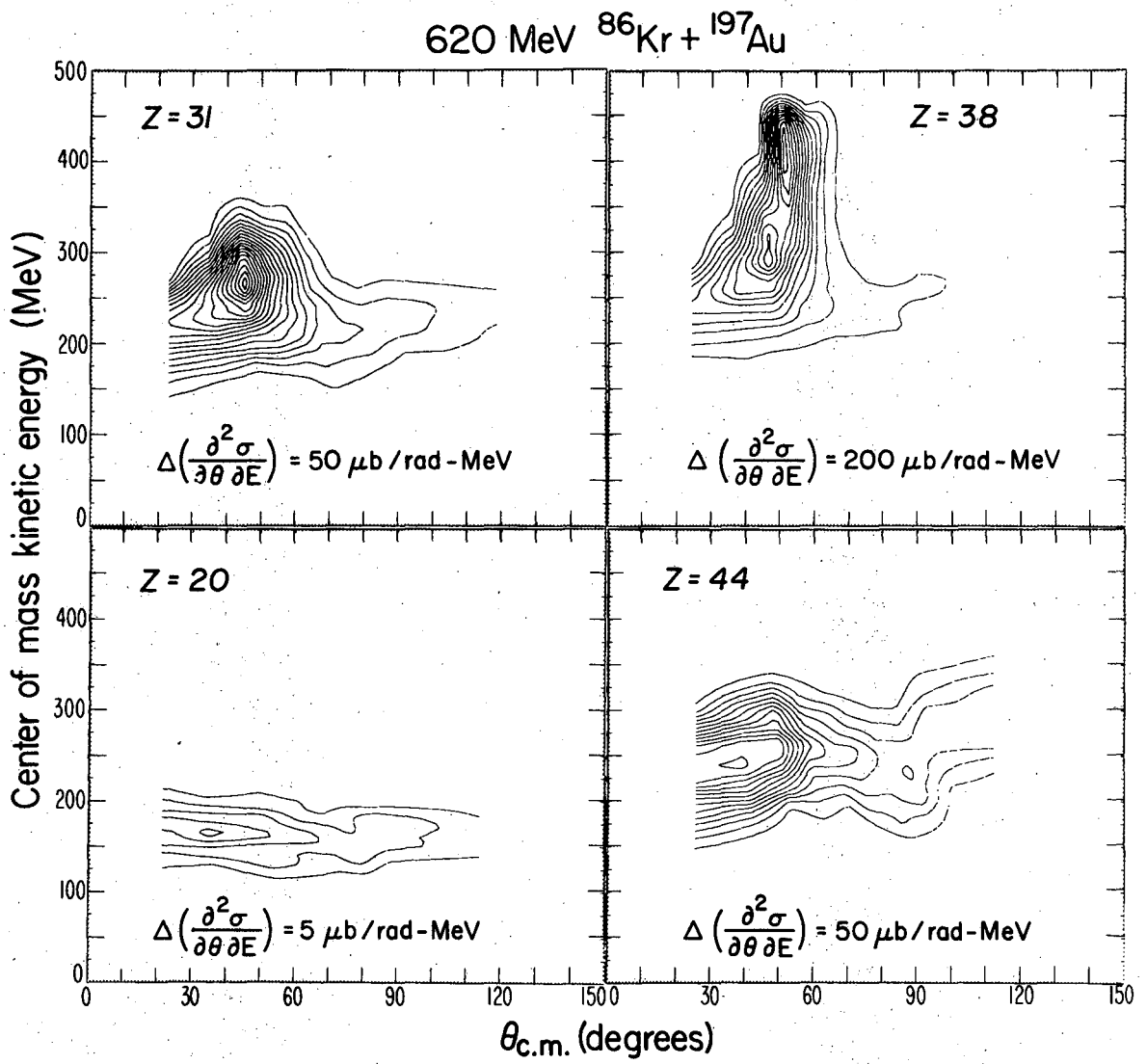

XBL 761-2089

Fig. 23

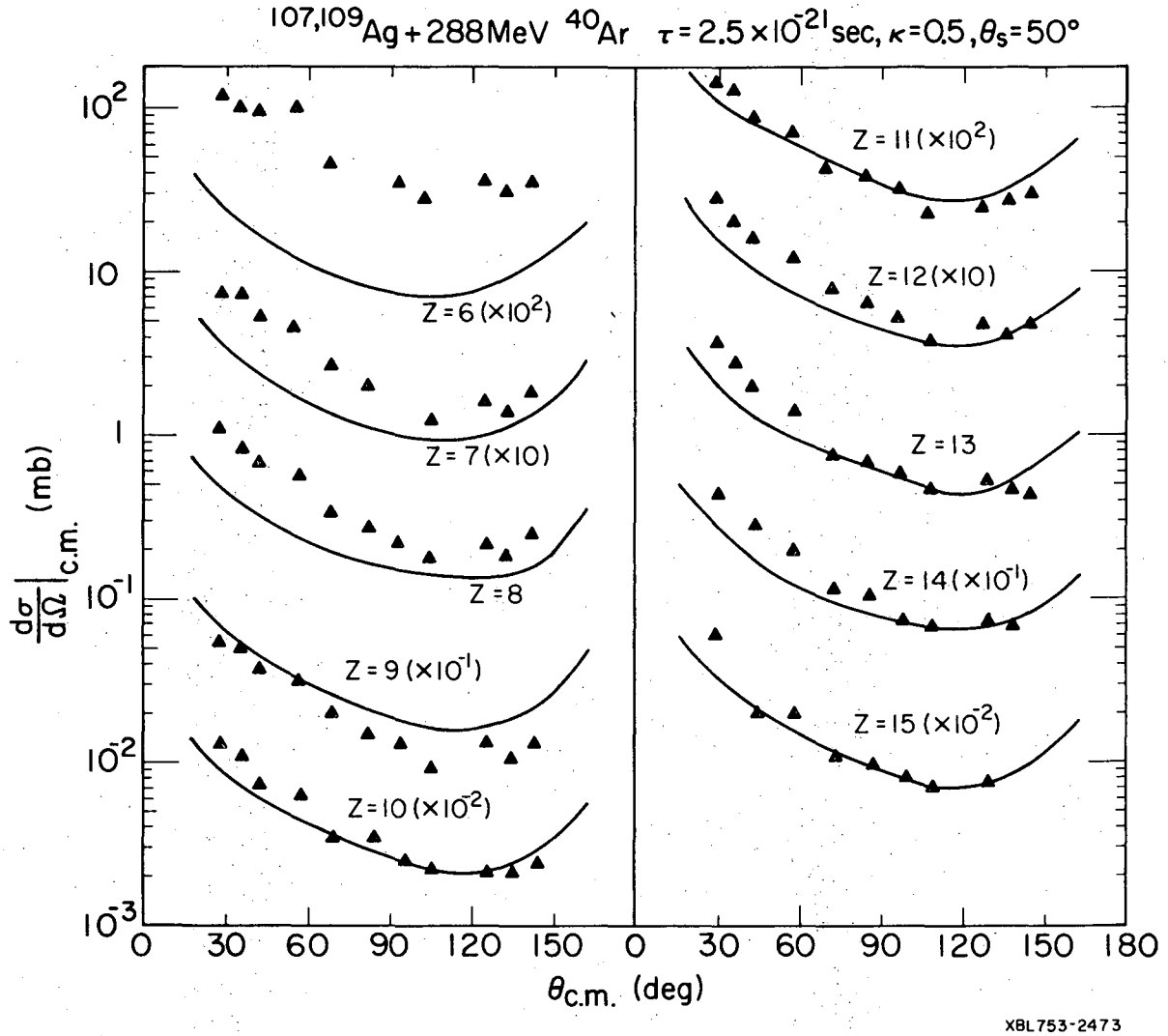
107,109Ag + 288MeV 40Ar τ = 2.5×10⁻²¹ sec, κ=0.5, θs=50°
Z = 6 (×10²)
Z = 7 (×10)
Z = 8
Z = 9 (×10⁻¹)
Z = 10 (×10⁻²)
Z = 11 (×10²)
Z = 12 (×10)
Z = 13
Z = 14 (×10⁻¹)
Z = 15 (×10⁻²)
dσ/dΩ|c.m. (mb)
θc.m. (deg)
XBL753-2473

Fig. 24

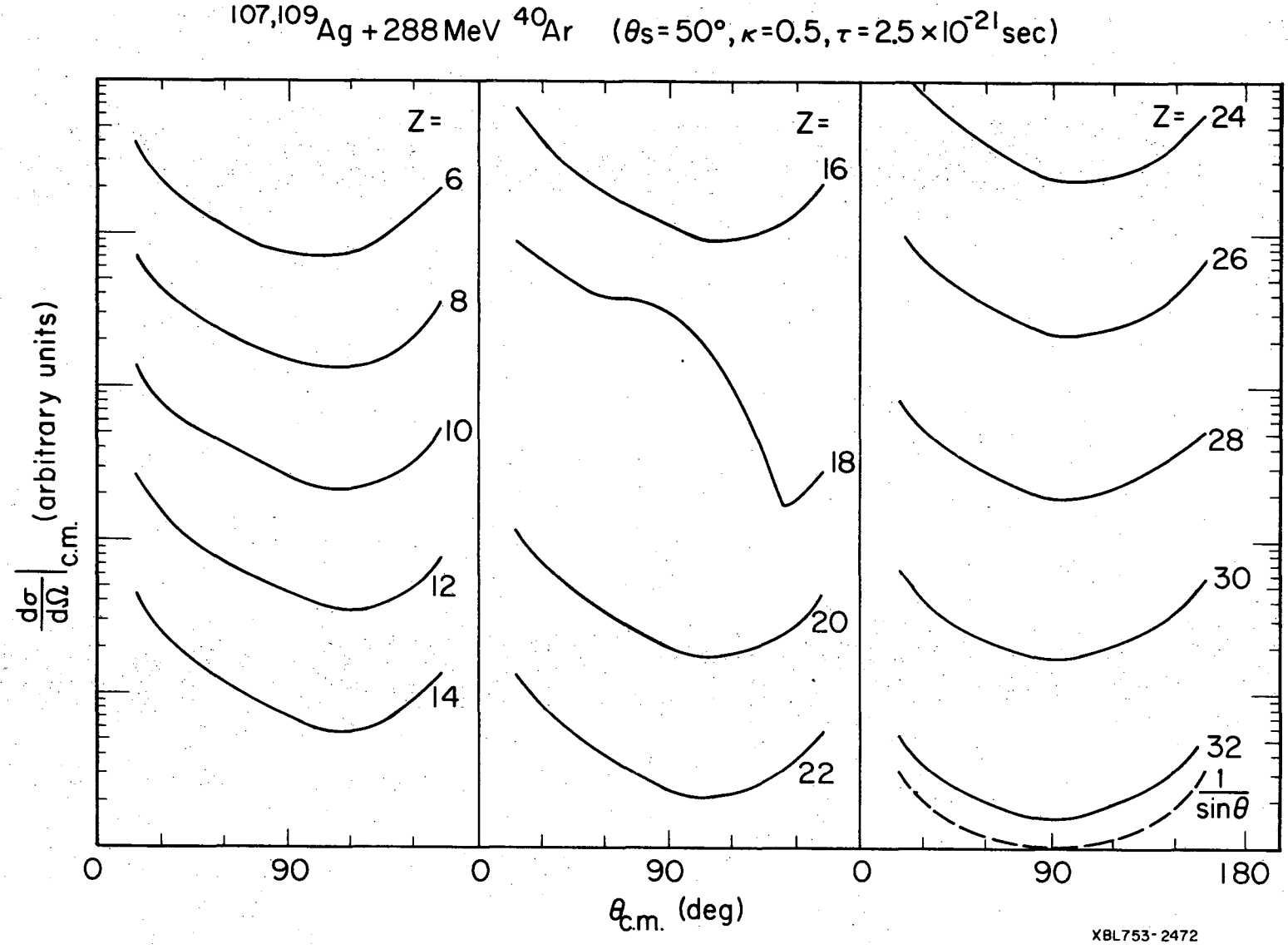

Fig. 25

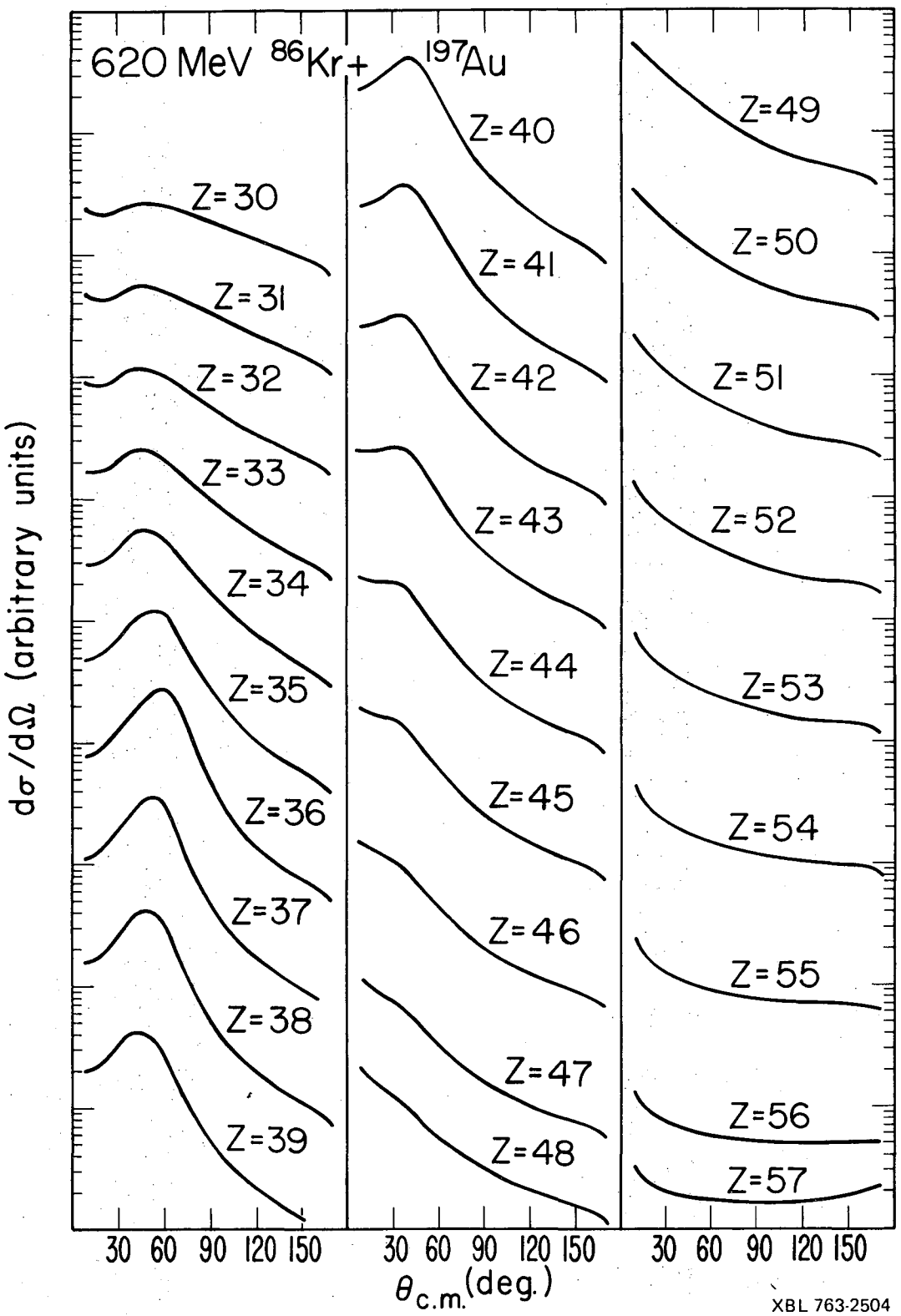
620 MeV 86Kr+ 197Au
Z=30
Z=31
Z=32
Z=33
Z=34
Z=35
Z=36
Z=37
Z=38
Z=39
Z=40
Z=41
Z=42
Z=43
Z=44
Z=45
Z=46
Z=47
Z=48
Z=49
Z=50
Z=51
Z=52
Z=53
Z=54
Z=55
Z=56
Z=57
dσ/dΩ (arbitrary units)
30 60 90 120 150
30 60 90 120 150
30 60 90 120 150
θc.m.(deg.)
XBL 763-2504

Fig. 26

TECHNICAL INFORMATION DIVISION
LAWRENCE BERKELEY LABORATORY
UNIVERSITY OF CALIFORNIA
BERKELEY, CALIFORNIA 94720